Chronic Intermittent Hypoxia reveals role of the Postinspiratory Complex in swallow pattern generation

Alyssa Huff[1], Marlusa Karlen-Amarante[1], Luiz Marcelo Oliveira[1], Jan Marino Ramirez[1,2]

[1]Center for Integrative Brain Research, Seattle Children's Research Institute, Seattle, WA, 98101
[2]Department of Neurological Surgery, University of Washington School of Medicine, Seattle, WA, USA, 98108

Corresponding Author
Jan Marino Ramirez, PhD
Seattle Children's Research Institute
1900 9th Avenue Seattle WA 98101
Tel (206) 884-8188
Jan.ramirez@seattlechildrens.org

Author Contributions: A.H., M.K.A., L.M.O. and J.M.R. designed research; A.H. and M.K.A., L.M.O. performed research; A.H., M.K.A., and L.M.O. analyzed data; and A.H., L.M.O., J.M.R. wrote the paper.

Keywords: medullary circuitry, rhythm generation, airway protection, laryngeal adductor reflex

This PDF file includes:

Main Text
Figures 1-4
Supplemental Figure 1-3
Tables S1-4

Abstract

Obstructive sleep apnea (OSA) is a prevalent sleep-related breathing disorder that results in multiple bouts of intermittent hypoxia. OSA has many neurologic and systemic comorbidities including dysphagia, or disordered swallow and discoordination with breathing. However, the mechanism in which chronic intermittent hypoxia (CIH) causes dysphagia is unknown. Recently we showed the Postinspiratory complex (PiCo) acts as an interface between the swallow pattern generator (SPG) and the inspiratory rhythm generator, the preBötzinger Complex, to regulate proper swallow-breathing coordination (A. D. Huff et al., 2023). PiCo is characterized by interneurons co-expressing transporters for glutamate (Vglut2) and acetylcholine (ChAT). Here we show that optogenetic stimulation of ChATcre:Ai32, Vglut2cre:Ai32, and ChATcre:Vglut2FlpO:ChR2 mice exposed to CIH does not alter swallow-breathing coordination, but unexpectedly the generation of swallow motor pattern was significantly

disturbed. This suggests, glutamatergic-cholinergic neurons in PiCo are not only critical for the gating of postinspiratory and swallow activity, but also play important roles in the generation of swallow motor pattern. Our study also suggests that swallow disruption, as seen in OSA involves central nervous mechanisms interfering with the generation of the swallow pattern and laryngeal activation. These findings are crucial for understanding the mechanisms underlying dysphagia in OSA and other breathing and neurological disorders.

Introduction

Obstructive sleep apnea (OSA) is highly prevalent and a major public health concern (Chang et al., 2023; McNicholas et al., 2015; Phillipson, 1993; J. M. Ramirez et al., 2013; Roberts et al., 2022; Wright & Sheldon, 1998). It is characterized by frequent bouts of apnea during sleep caused by pharyngeal collapse, resulting in multiple bouts of hypoxia referred to as chronic intermittent hypoxia (CIH). CIH increases the gain of the carotid body (CB) response to hypoxia which seems to be a major cause for the multiple comorbidities of OSA (Iturriaga, 2023; Prabhakar et al., 2023). These OSA-related comorbidities (Pack, 2023) include an increase in mortality (Vgontzas et al., 2023) and cancer risk (Sánchez-de-la-Torre et al., 2023), increased arousal and sleep fragmentation (Horner, 2023), increased sympathetic drive leading to cardiovascular disease; metabolic syndromes such as obesity and diabetes (Kurnool et al., 2023), renal disease, asthma, (Bonsignore et al., 2019), and decreased cognition (Brockmann & Gozal, 2022). OSA is also commonly associated with dysphagia, disordered swallow function (Pizzorni et al., 2021; Schindler et al., 2014). Clinical studies have begun to investigate physiologic parameters of OSA-related dysphagia, but little is known about the underlying mechanisms.

CIH and the increased gain in CB activity lead to disturbances in multiple neuronal mechanisms originating in the central nervous system (Arias-Cavieres et al., 2021; Arias-Cavieres et al., 2020; da Silva et al., 2021; Domingos-Souza et al., 2021; Jia et al., 2022; David D Kline, 2010; David D Kline et al., 2019; Lin et al., 2007; Marciante et al., 2021; J.-M. Ramirez et al., 2020; Souza et al., 2019). CIH directly affects neuronal network functions within the ventral respiratory column (VRC), in particular the preBötzinger complex (preBötC) (Garcia et al., 2017; Garcia et al., 2016), a critical rhythmogenic network implicated in swallow-breathing coordination (A. Huff et al., 2022).

Swallow share anatomical structures with breathing and it is critical these two behaviors are coordinated to prevent aspiration of food/liquid into the airway. Dysphagia, or disruption of swallow and discoordination with breathing, is directly linked to altered quality of life and failure to thrive in respiratory related diseases not only in OSA (Bhutada et al., 2020; Kato et al., 2016; Pizzorni et al., 2021; Schindler et al., 2014), but also chronic obstructive pulmonary disease (COPD) (Garand et al., 2018; Ghannouchi et al., 2016; Nagami et al., 2017), and neurodegenerative diseases such as Parkinson's disease, Alzheimer disease, and motor neuron diseases (Walshe, 2014).

Swallow-breathing coordination depends on the precise temporal activation of the pharyngeal and laryngeal muscles, as well as muscles involved in respiratory control. This coordination is controlled by various regions throughout the brainstem. The generation of swallow is thought to be governed by the caudal portion of the nucleus tractus solitaries (cNTS), specifically the interstitial and intermediate portions (Altschuler et al., 1989; J. Kessler & A. Jean, 1985; J. P. Kessler & A. Jean, 1985). Swallow predominately occurs during a respiratory phase referred to as postinspiration, the transitory phase from inspiration to expiration (A. D. Huff et al., 2023). Thus, activity in the cNTS must be coordinated with the inspiratory rhythm generator, the preBötC, and the postinspiratory rhythm generator, the postinspiratory complex (PiCo), to prevent swallows from occurring during inspiration increasing the risk for aspiration.

Recently published studies have demonstrated that PiCo acts as a gate for swallow and laryngeal postinspiratory behaviors and aids in the proper coordination and timing for swallow and breathing (Ain Summan Toor et al., 2019; A. D. Huff et al., 2023). In the present study we explored the effects of CIH on PiCo and its role in coordinating swallowing and breathing in order to understand how OSA and other disorders associated with intermittent hypoxia (e.g. epilepsy, Rett Syndrome) lead to dysphagia. Building on the experiments preformed in our control cohort (A. D. Huff et al., 2023) we studied the impact of CIH using an established mouse model for OSA (Garcia et al., 2017; Garcia et al., 2016; A. Huff et al., 2022; Peng & Prabhakar, 2004; Peng et al., 2021). Similar to our control model, optogenetic stimulation of PiCo in ChATcre:Ai32, Vglut2cre:Ai32, and ChATcre:Vglut2FlpO:ChR2 mice stimulated both swallow and laryngeal activation. Unexpectedly, we find that PiCo-triggered swallow-breathing coordination itself is not altered, rather the alteration is in the swallow motor pattern. We

propose that PiCo is directly involved in swallow pattern generation and CIH disrupts the connection between PiCo and the swallow pattern generator (SPG).

Results

Optogenetic stimulation of neurons in PiCo region

We confirmed that optogenetic stimulation of PiCo neurons triggers swallow and laryngeal activation similar to the control mice exposed to room air (A. D. Huff et al., 2023). However, when exposed to CIH, optogenetic stimulation of ChATcre:Vglut2FlpO:ChR2 neurons triggered a variety of abnormal swallow motor patterns (Figure 1B). Only 6% of all PiCo-triggered swallows could be characterized as normal, classic swallows (Figure 1Bi), while the vast majority of swallow motor patterns had a-typical shapes and temporal sequences. We characterized these atypical swallow patterns as follows: 1) Non-classic swallow, 28%: submental and laryngeal shape, onset, and offset are similar (Figure 1Bii). 2) Tonic pre-swallow, 41%: low amplitude tonic activity of the submental and laryngeal complexes during the laser pulse with a swallow immediately following (Figure 1Biii). 3) Laryngeal adductor reflex (LAR) + swallow 4%: quick burst of submental and laryngeal complex followed by a short quiescence in activity then a swallow (Figure 1Biv). 4) Non-LAR + swallow, 21%: quick burst of submental and laryngeal complex followed by low amplitude activity merging into a swallow (Figure 1Bv). A mixed-effects ANOVA detected a significant effect due to stimulation duration (p-value = 0.03), however Tukey's multiple comparisons test revealed no significant differences in behavior duration across stimulation durations (Figure 1E). Regardless of the motor pattern, swallow duration is independent of laser pulse duration, each are considered a swallow and will be grouped as swallows for further analysis.

We also observed differences in laryngeal activation when exposed to CIH. Optogenetic stimulation of ChATcre:Vglut2FlpO:ChR2 neurons did not stimulate laryngeal activation in 3 of the 11 mice. In the 8 mice where laryngeal activation was stimulated, a burst of submental complex activity was present during PiCo-stimulated laryngeal activation in 7 mice, while one mouse had a low amplitude tonic activity (Figure 2). Looking back to the control mice exposed to room air, only 1 out of 7 mice had a burst of submental complex activity, 4 mice had a low tonic submental complex activity and 2 mice had no submental activity (A. D. Huff et al., 2023).

A mixed-effects ANOVA detected a significant effect on laryngeal activation duration due to stimulation duration (*p*-value = 0.01) in CIH conditions. Tukey's multiple comparisons test revealed significant differences ($p < 0.05$) between 40ms and 80ms, 120ms, 160ms and 200ms indicating laryngeal activation duration is dependent on laser pulse duration (Figure 2C).

Probability of triggering a swallow

We next compared the probability of triggering a swallow between all three genetic types exposed to CIH. There were no PiCo-triggered swallows in 4 out of 14 mice in response to optogenetic stimulation of ChATcre:Ai32. In Vglut2cre:Ai32, no PiCo-triggered swallows in 3 out of 11 mice. However, stimulation of ChATcre:Vglut2FlpO:ChR2 neurons triggered a swallow in all 11 mice.

A two-way ANOVA test revealed a significant difference between temporal characteristics and the genetically defined neuron type ($p<0.0001$, df= 4, F= 17.37) in ChATcre:Ai32 (N=14), Vglut2cre:Ai32 (N= 11), and ChATcre:Vglut2:ChR2 (N= 11) when looking at the probability of triggering a swallow (Figure 3A). A post-hoc Tukey's multiple comparison test revealed there is no difference in the probability of triggering a swallow between ChATcre:Ai32 and Vglut2cre:Ai32 mice. However, there in an increased probability of triggering a swallow when ChATcre:Vglut2FlpO:ChR2 neurons are activated within 50%, (p= 0.04), 70% (p= 0.03), and 90% (p= 0.02) of the respiratory cycle compared to ChATcre:Ai32. There is also an increased probability of triggering a swallow when ChATcre:Vglut2FlpO:ChR2 neurons are activated at all phases of the respiratory cycle: 10%, (p= 0.03), 30% (p= 0.04), 50% (p= 0.02), 70% (p= 0.02), and 90% (p= 0.01) compared to Vglut2cre:Ai32. Whereas under control conditions, when mice were exposed to room air, we found no significant difference in the probability of triggering a swallow between ChATcre:Ai32, Vglut2:Ai32, and ChATcre:Vglut2FlpO:ChR2 mice (A. D. Huff et al., 2023).

Probability of triggering laryngeal activation

Optogenetic stimulation of ChATcre:Ai32 and Vglut2:Ai32 neurons stimulated laryngeal activation in all mice exposed to CIH. However, in ChATcre:Vglut2FlpO:ChR2 CIH mice,

laryngeal activation was never stimulated in 3 out of 11 mice. By contrast in control, laryngeal activation was stimulated in all ChATcre:Vglut2FlpO:ChR2 mice (A. D. Huff et al., 2023).

A two-way ANOVA test revealed a significant difference between temporal characteristics and the genetically defined neuron type ($p<0.0001$, df= 4, F= 31.98) in ChATcre:Ai32, Vglut2cre:Ai32, and ChATcre:Vglut2FlpO:ChR2 CIH-exposed mice with regards to the probability of triggering laryngeal activation (Figure 3A). A post-hoc Tukey's multiple comparison test revealed there is no difference in the probability of triggering laryngeal activation between Vglut2cre:Ai32 and ChATcre:Vglut2FlpO:ChR2 CIH-exposed mice. Whereas in control conditions Vglut2cre:Ai32 had a lower probability of stimulating laryngeal activation than ChATcre:Vglut2FlpO:ChR2 mice (A. D. Huff et al., 2023). There is an increased probability of triggering laryngeal activation when ChATcre:Ai32 neurons are activated within 50%, ($p= 0.03$), 70% ($p= 0.0002$), and 90% ($p<0.0001$) of the respiratory cycle compared to Vglut2cre:Ai32 CIH-exposed mice. There is an increased probability of triggering laryngeal activation when ChATcre:Ai32 neurons are activated at all phases of the respiratory cycle: 10%, ($p= 0.03$) 30% ($p= 0.002$), 50% ($p= 0.002$), 70% ($p= 0.01$), and 90% ($p= 0.05$) compared to ChATcre:Vglut2FlpO:ChR2 CIH-exposed mice. By contrast, in control conditions there was no difference in the probability between ChATcre:Ai32 and ChATcre:Vglut2FlpO:ChR2 mice (A. D. Huff et al., 2023).

PiCo phase-dependent response

Stimulation of ChATcre:Ai32 neurons in PiCo region triggers a swallow or stimulates laryngeal activation in a respiratory phase-dependent manner. However, this stimulation-evoked phase dependency differs among the three CIH-exposed genetically defined neuron types.

A two-way ANOVA test revealed a significant interaction between time and behavior ($p<0.0001$, df= 4, F= 10.99) in ChATcre:Ai32, Vglut2cre:Ai32, and ChATcre:Vglut2:ChR2 mice (Figure 3B). A post-hoc Tukey's multiple comparison test revealed laryngeal activation is stimulated with a significantly higher probability when CIH-exposed ChATcre:Ai32 neurons are activated at 50% ($p= 0.0005$), 70% ($p<0.0001$), and 90% ($p<0.0001$) of the respiratory cycle. Laryngeal activation is stimulated with a significantly higher probability when CIH-exposed Vglut2cre:Ai32 neurons are activated at 70% ($p= 0.03$) of the respiratory cycle. However, swallow is triggered with a significantly higher probability when CIH-exposed

ChATcre:Vglut2FlpO:ChR2 neurons are activated within the first 10% (p= 0.004) and 30% (p= 0.001) of the respiratory cycle. However, under control, normoxic conditions in ChATcre:Vglut2FlpO:ChR2 we did not find a significant difference in the first 10% and 30% of the respiratory cycle, rather a significant increase in the probability that laryngeal activation would be stimulated within 70% and 90% of the respiratory cycle (A. D. Huff et al., 2023).

Respiratory response to optogenetic stimulation of PiCo

We divided PiCo stimulated responses into either swallow or non-swallow (Figure 3-figure supplement 1). Stimulation of PiCo neurons that resulted in either laryngeal activation or in a "no-motor response" were considered non-swallows. Using a Pearson correlation and simple linear regression, the correlation coefficient (r, Figure 3- figure supplement 1A) and line of best fit (slope, Figure 3- figure supplement 1B), respectively, was calculated for each CIH exposed genetic mouse type and response to determine the degree of correlation between behavior response and reset of the respiratory rhythm. This test reveals that there is a high degree of correlation between shifting or delaying the following inspiratory burst and triggering a swallow when stimulating ChATcre:Ai32 ($r = 0.76$, $p< 0.0001$, slope= 0.75), Vglut2cre:Ai32 ($r = 0.71$, $p< 0.0001$, slope= 0.82) and, ChATcre:Vglut2FlpO:ChR2 ($r = 0.79$, $p< 0.0001$, slope= 0.79) CIH-exposed mice. Under control, normoxic conditions we found a high degree of correlation between shifting or delaying the following inspiratory burst and triggering a swallow when stimulating ChATcre:Ai32, and ChATcre:Vglut2FlpO:ChR2 mice, while only a moderate degree of correlation in Vglut2cre:Ai32 mice (A. D. Huff et al., 2023). This suggest that triggering a swallow in each genetic type has a strong effect on resetting the respiratory rhythm and is strengthened or not altered in CIH conditions.

We found a moderate degree of correlation between the following inspiratory burst and non-swallows stimulated in ChATcre:Ai32 ($r = 0.36$, $p< 0.0001$, slope= 0.16), and a low degree of correlation in Vglut2cre:Ai32 ($r = 0.22$, $p< 0.0001$, slope =0.17) and ChATcre:Vglut2FlpO:ChR2 ($r = 0.28$, $p= 0.0001$, slope= 0.18) mice. Under control, normoxic conditions we found a moderate degree of correlation between shifting or delaying the following inspiratory burst and stimulating non-swallows when stimulating ChATcre:Ai32 mice and a low degree of correlation in Vglut2cre:Ai32 and ChATcre:Vglut2FlpO:ChR2 mice (A. D. Huff et al., 2023). This suggests that triggering a swallow has a stronger effect on resetting the respiratory

rhythm than activating non-swallows in all the genetic mouse types, which is not altered by CIH exposure.

Swallow-related characteristics in water-triggered and PiCo-triggered swallows

Figure 1A depicts the swallow motor patterns of a water-evoked swallow and 1B of various swallow motor patterns of PiCo-evoked swallow. A mixed-effect ANOVA revealed no significant difference in swallow onset relative to inspiratory onset (Figure 1- figure supplement 1A) and swallow onset relative to inspiratory peak (Figure 1- figure supplement 1B) between PiCo-evoked and water-evoked swallows in CIH-exposed mice. This was also found under control conditions (A. D. Huff et al., 2023). We were unable to perform a repeated measures ANOVA due to swallows not being triggered by PiCo stimulation in some mice, as mentioned above. All water- and PiCo-triggered swallow-related characteristics in all three CIH-exposed genetic mouse lines are reported in Table S1.

PiCo-triggered swallows are characterized by a significant decrease in duration compared to swallows evoked by water in ChATcre:Ai32 (265 ± 132ms vs 144 ± 101ms; paired t-test: p= 0.0001, t= 5.21, df= 8), Vglut2cre:Ai32 (308 ± 184ms vs 125 ± 44ms; paired t-test: p= 0.0003, t= 6.46, df= 7), and ChATcre:Vglut2FlpO:ChR2 (230 ± 67ms vs 130 ± 35ms; paired t-test: p= 0.0005, t= 5.62, df= 8) CIH-exposed mice (Table S1).

PiCo-triggered swallows have a significant decrease in submental amplitude compared to swallows evoked by water in ChATcre:Ai32 (91 ± 7 vs 38 ± 35 % of max; paired t-test: p= 0.002, t= 4.91, df= 7), Vglut2cre:Ai32 (84 ± 10 vs 45 ± 32 % of max; paired t-test: p= 0.006, t= 3.84, df= 7), and ChATcre:Vglut2FlpO:ChR2 (88 ± 10 vs 39 ± 22 % of max; paired t-test: p= 0.001, t= 7.47, df= 8) CIH-exposed mice (Table S1).

Sex-specific differences in swallows triggered by optogenetic stimulation of PiCo region

All water- and PiCo-triggered sex-specific swallow-related characteristics in all three CIH-exposed genetic mouse lines are reported in Table S2-4. In ChATcre:Ai32 female mice, PiCo-triggered swallow onset relative to inspiratory onset occurs later in the respiratory cycle (0.31 ± 0.04 vs 0.37 ± 0.04; paired t-test: p= 0.04, t= 2.38, df= 8). There are no sex-specific differences in PiCo-triggered swallows in Vglut2cre:Ai32 or ChATcre:Vglut2FlpO:ChR2 CIH-exposed mice.

Neuroanatomy of PiCo transfection

Post-hoc histological analysis was performed in the double conditioned ChATcre:Vglut2FlpO:ChR2 mouse to check the transfection of PiCo neurons after injection of the pAAV-hSyn Con/Fon hChR2(H134R)-EYFP vector (ChATcre:Vglut2FlpO:ChR2) (Figure 4). NAmb cholinergic neurons had no transfection and the rostrocaudal distribution of the transgene-expressing neurons was analyzed. Eleven ChATcre:Vglut2FlpO:ChR2 mice were stimulated and triggered a swallow, while laryngeal activation was triggered in only 8 mice. In all 11 CIH-exposed mice we found that 155 ± 9 SEM neurons expressed EYFP (Figure 4). While in the control conditions we found that 133 ± 9 SEM neurons expressed EYFP (A. D. Huff et al., 2023). In the CIH-exposed mice we had high bilateral transfection of ChR2 into PiCo neurons ranging from 121-189 neurons with one animal having 88 neurons. The animal with 88 neurons did not appear to have a different optogenetic response compared to the other animals.

Discussion

In mice, and other mammals including humans, exposed to room air, swallow related muscles follow a stereotypic, rostro-caudal sequential muscle pattern activation (J. Basmajian & Dutta, 1961; Doty & Bosma, 1956; Pitts & Iceman, 2023). The activation pattern must be precisely timed and shaped in order to guarantee that food and liquid particles are guided into the esophagus and ultimately the digestive system, rather than the lungs. Disturbances in any aspect of the swallow patterning leads to aspiration resulting in the penetration of food or liquid through the vocal folds, entering the lungs. In the long-term, aspiration may lead to aspiration pneumonia. We found that after exposure to CIH only 6% swallows triggered by optogenetic stimulation of PiCo, specifically the ChATcre:Vglut2FlpO:ChR2 neurons, followed this classic swallow motor pattern (Figure 1Bi). While 28% of PiCo-triggered swallows lost important characteristics of the sequential motor activation crucial for proper bolus transport (Pitts & Iceman, 2023). In these “non-classic swallows” the submental and laryngeal muscles were activated simultaneously, which could impair the effective transport of food from the oral cavity into the esophagus and digestive system. Stimulation of glutamatergic/cholinergic neurons also induced “tonic pre-swallow” activity of both the submental and laryngeal complexes prior to triggering a swallow in 41% of PiCo-triggered swallows. The functional significance of this tonic activity cannot be assessed in our animal model.

Interestingly, the respiratory phase in which swallow and laryngeal activation was triggered by PiCo stimulation remained the same, compared to control conditions, suggesting that after CIH swallow disruption mediated by PiCo activation is not primarily caused by swallow-breathing discoordination (Figure 3). Interestingly, we did not see any changes in the reset properties of the respiratory rhythm compared to control conditions (Figure 3-figure supplement 1). We also observed no differences between the water-triggered swallow onset and PiCo-triggered swallow onset in relation to inspiration onset and peak inspiration (Figure 1-figure supplement 1). Thus, CIH does not alter PiCo's ability to act as a gate and coordinate the timing for swallow and breathing. Rather, our data reveals CIH disrupts swallow pattern generation likely due to changes in the interaction between PiCo and the SPG, presumably the cNTS. While it has previously been demonstrated that PiCo acts as a gate for swallow initiation and an important hub in swallow-breathing coordination (A. D. Huff et al., 2023), previous studies did not clearly demonstrate that PiCo is involved in swallow pattern generation itself. Thus, here we show for the first time that CIH resulted in the instability of the swallow motor pattern activated by stimulating PiCo, suggesting PiCo plays a role in swallow pattern generation.

Under control conditions, there is no statistical difference in the probability of triggering a swallow during optogenetic stimulation of ChATcre:Ai32, Vglut2cre:Ai32 and ChATcre:Vglut2FlpO:ChR2 neurons. However, when exposed to CIH, ChATcre:Ai32 and Vglut2:Ai32 mice have a lower probability of triggering a swallow -- in some mice swallow was never triggered – compared to the ChATcre:Vglut2FlpO:ChR2 mice. By contrast the ChATcre:Vglut2FlpO:ChR2 mice have a lower probability of triggering laryngeal activation than the ChAtcre:Ai32 mice. This suggests that CIH has differential effects on neurons that only express ChAT and Vglut2 versus the PiCo-specific interneurons that co-express ChAT and Vglut2, emphasizing the importance of targeting and manipulating these PiCo-specific interneurons.

Variability to swallow motor pattern

Previously we suggested that the PiCo-evoked laryngeal activation could be a central and integral component to a laryngeal adductor reflex (LAR) (A. D. Huff et al., 2023). However, there had been no reports of centrally evoked LAR or an LAR independent of mechanical, electrical, or chemical peripheral stimulation or swallow. Here we show, for the first time,

optogenetic stimulation of PiCo, in mice exposed to CIH, triggers swallow-related LAR (Figure 1Biv). The afferent limb of the LAR is governed by the superior laryngeal nerve (SLN) where sensory impulses travel through the nodose ganglion and terminate on the cNTS (Sessle, 1973). It is likely that both swallow and LAR involves interneurons of the solitarius-ambiguus pathway, possibly activated by PiCo stimulation.

In addition to the classic LAR response, PiCo stimulation also triggered non-LAR swallows (Fig. 1Bv). To be considered an LAR there must be a quiescence period of laryngeal activity between the reflex and the swallow (Ambalavanar et al., 2004; Ludlow et al., 1992). In these swallows there was a convergence of the initial laryngeal peak and augmenting swallow-related laryngeal activity. The functional merging of these two activity patterns is not understood. It has been shown that excessive or inappropriate laryngeal activity could lead to functional disorders or life-threatening conditions (Sun et al., 2011), such as obstructive apnea, spasmodic dysphonia, asphyxia, sudden infant death syndrome (SIDS) and aspiration pneumonia (Ikari & Sasaki, 1980; Ludlow et al., 1995; Thompson et al., 2005). While we are unable to evaluate the functional significance of the variable swallow motor patterns triggered by PiCo in this study, we previously reported CIH causes a disruption in swallow motor pattern with a delay in swallow-related laryngeal activation (A. Huff et al., 2022). Further dynamic analysis of muscle pattern activation in control and CIH exposed mice is necessary to understand the functional differences of this variable muscle pattern activation.

Our study indicates that PiCo neurons are highly integrated with the overall swallow motor pattern. Variability in response to CIH on swallow motor pattern is reminiscent to the increased variability also seen in the generation of the respiratory motor pattern (Garcia et al., 2017; Garcia et al., 2016). While it is possible that portions of the presumed SPG remain less affected by CIH, which could offset these instabilities in order to produce functional swallows, our data suggest that PiCo targets microcircuits within the SPG that are highly affected by CIH. The NTS is a primary first site for upper airway and swallow-related sensory termination in the brainstem (Jean, 1984). It has been shown that CIH induces changes to the cardio-respiratory sensory processing portion of the NTS, resulting in an increase in cNTS neuronal activity (David D Kline, 2010; D. D. Kline et al., 2007). Targeting this swallow microcircuit via activation of only one PiCo-related neuron type, ChAT or Vglut2, does not reliably trigger swallows under CIH conditions, unlike control room air conditions (A. D. Huff et al., 2023). To understand the

complex disruption of CIH on swallow pattern generation it is important to note that we are measuring changes in two muscle complexes which spread among three motor neuron pools: hypoglossal nucleus, trigeminal nucleus, and nucleus ambiguus (Badran et al., 2005; Bieger & Neuhuber, 2006; Kemplay & Cavanagh, 1983; Razlan et al., 2018).

Variability to laryngeal activation motor pattern

We observed a shift in the dominance of "laryngeal activation" submental complex motor activity pattern. Under control conditions optogenetic stimulation of ChATcre:Vglut2FlpO:ChR2 neurons resulted in laryngeal activation with 3 types of submental activation: tonic, burst, and no activation; with the majority of mice having tonic submental activation (Figure 2B). However, when exposed to CIH, 7 out of 8 mice had burst submental activation. This is consistent with the known increased activity of pharyngeal dilator muscles in OSA patients (Mezzanotte et al., 1992; Saboisky et al., 2012) and in CIH animal models (Kubin, 2019). This could constitute a compensatory mechanism to keep the airway patent (Dempsey et al., 2010).

It has been noted that acute bouts of hypoxia reduce the excitability of laryngeal adductor neurons, suggesting a "fail-safe" mechanism that in the presence of hypoxia, laryngeal closure is prevented (Ikari & Sasaki, 1980). However, this does not seem to be the case with chronic intermittent hypoxia. Severity of OSA is correlated to impairments of laryngeal mucosal function, suggesting reasons for blunted airway protective mechanisms (Nguyen et al., 2005). Here we use a model of severe OSA, which results in an over-excitation in central laryngeal activity.

Limitations

The use of anesthesia continues to be an unavoidable limitation for this preparation. There were 2 mice that did not swallow in response to water stimulation, most likely due to anesthetic depth. In this preparation we are unable to directly determine the functionality of the variable swallow motor pattern seen after CIH. This limits our ability to make direct comparisons between dysphagic swallows in OSA patients. These limitations are a trade-off for the unique advantages of manipulating specific genetically defined neuron types under *in vivo* conditions to assess neuronal alterations in OSA related dysphagia.

Conclusion

Clinical dysphagia is typically seen in OSA, and other disorders associated with CIH. OSA related dysphagia has been characterized as a delayed swallow reflex, decreased time between swallow and initiation of the next inspiration, and disruption of the pharyngeal phase of swallow (Levring Jaghagen et al., 2003; Teramoto et al., 1999; Valbuza et al., 2011). Using an *in vivo* mouse model we recently described that CIH delays swallow-related laryngeal activation which increases the risk for foreign materials to enter into the airway (aspiration) instead of the esophagus (A. Huff et al., 2022). Here we show that PiCo, a neuronal network which is critical for the generation of postinspiratory activity (Andersen et al. 2016) and implicated in the gating of swallowing (Huff, 2023), is severely affected by CIH. Stimulating PiCo-specific interneurons after CIH exposure evoked swallows characterized by abnormal swallow motor patterns, while the swallow-breathing coordination was relatively unaffected. The severe disruption in the precise temporal sequences of swallows evoked by PiCo stimulation after CIH exposure has important implications for understanding the mechanisms underlying dysphagia. Our data suggest that PiCo is not only a neuronal structure critical for gating postinspiratory and swallowing activity, but also critical for the generation of swallowing itself. To the best of our knowledge, no microcircuit has previously been identified that can directly impact the generation of the swallow motor pattern itself. Swallows are characterized by a very robust, yet complex stereotypic motor sequence that is typically triggered in an all-or-none manner. The strict temporal sequence of this motor pattern is critical for allowing the physiological transport of food to reach the digestive system. Any disturbance in this sequence has detrimental consequences including aspiration, the leading cause of death in many neurodegenerative diseases. Our study also suggests that swallow disruption, as seen in OSA, may not primarily be due to the swallow-breathing discoordination, but rather involve a central nervous dysfunction of the swallow pattern and laryngeal activation.

Methods

Animals

Adult (P51-148, average P76) male and female mice were bred at Seattle Children's Research Institute (SCRI) and used for all experiments. Vglut2-IRES-cre and ChAT-IRES-cre homozygous breeder lines were obtained from Jackson laboratories (stock numbers 028863 and

031661, respectively). Cre mice were crossed with homozygous mice containing a floxed STOP channelrhodopsin-2 fused to an EYFP (Ai32) reporter sequence from Jackson laboratories (stock number 024109). Vglut2-IRES-cre crossed with Ai32 will be reported as Vglut2:Ai32 and the ChAT-IRES-cre crossed with Ai32 as ChAT:Ai32. ChAT-IRES-cre, and Vglut2- ChAT-IRES-cre 2-FlpO-D, *technically known as* 129S-Slc17a6$^{tm1.1(flpo)Hze}$/J was obtained from Jackson Laboratories (#031661 and #030212, respectively). To generate double-transgenic mice, the ChATcre and Vglut2FlpO strains were interbred to generate compound homozygotes, named as ChATcre:Vglut2FlpO $^{(+/+)}$, which tagged neurons that have a developmental history of expressing both ChAT and Vglut2. Mice were randomly selected from the resulting litters by the investigators. Offspring were group housed with ad libitum access to food and water in a temperature controlled (22 $\pm$ 1ºC) facility with a 12h light/dark cycle. All experiments and animal procedures were approved by the Seattle Children's Research Institute's Animal Care and Use Committee (IACUC #0058) and were conducted in accordance with the National Institutes of Health guidelines.

Brainstem injection of AAV

For the AAV injections, we target the PiCo neurons, as previously described (Anderson et al., 2016; A. D. Huff et al., 2023), and also confirmed by the present results (Figure 4). We restricted ChR2 expression to the PiCo region in order to transfect and photo-stimulate the region with the highest density of ChATcre:Vglut2FlpO neurons in PiCo region (Anderson et al., 2016). For AVV injection, the mice were anesthetized with isoflurane (2%). The correct plane of anesthesia was assessed by the absence of the corneal and hind-paw withdrawal reflexes. Mice received postoperative ketoprofen [7 mg/kg, subcutaneous (s.c.)] for two consecutive days. All surgical procedures were performed under aseptic conditions. The hair over the skull and neck were removed and skin disinfected. The mice were then placed prone on a stereotaxic apparatus (bite bar set at -3.5 mm for flat skull; David Kopf Instruments Tujunga, CA, USA). A 0.5 mm diameter hole was drilled into the occipital plate on both sides caudal to the parieto-occipital suture. Viral solutions were loaded into a 1.2 mm internal diameter glass pipette broken to a 20 μm tip (external diameter). To target the PiCo region with ChR2-AAV, the pipette was inserted in the brainstem in the following coordinates: 4.8 mm below the dorsal surface of the cerebellum, 1.1 mm lateral to the midline and 1.6 mm caudal to the lambda and bilateral

injections of 150 nL were made slowly at 50 nL/min, using a glass micropipette and an automatic nanoliter injector (NanoinjectII, Drummond Scientific Co. Broomall, PA). The mouse was allowed to recover for 3 days before beginning the chronic intermittent hypoxia protocol (see below).

The mouse strain containing ires-cre and ires-FlpO in $ChAT^+$ and $Vglut2^+$ respectively, had successful transfection of PiCo neurons by using a pAAV-hSyn Con/Fon hChR2(H134R)-EYFP adenovirus vector (cat# 55645-AAV8; AddGene, USA; abbreviated as AAV8-ConFon-ChR2-EYFP) herein named ChATcre:Vglut2FlpO:ChR2 in this study. This AAV is a cre-on/FlpO-on ChR2-EYFP under the synapsin promoter and encoded the photoactivatable cation channel channelrhodopsin-2 (ChR2, H134R) fused to EYFP. The vector was diluted to a final titer of 1 x 10^{13} viral particles/ml with sterile phosphate-buffered saline.

Chronic Intermittent Hypoxia

Mice of the ChATcre:Ai32, Vglut2cre:Ai32 and ChATcre:Vglut2FlpO:ChR2 were kept in collective cages with food and water *ad libitum* placed inside custom built chambers (volume: 185 liters) equipped with gas injectors as well as oxygen (O_2) sensors (Oxycycler, Huff Technologies Inc.). One chamber was used for CIH and the other for control. The CIH group was exposed to intermittent episodes of hypoxia, continuous injection of nitrogen (N_2) for 60 seconds, in order to reduce the percentage of inspired O_2 inside the chamber from 21% to 4.5-5%. Then continuous injection of compressed air for 5 minutes into the chamber to return the percentage of O_2 to 21% before the start of a new hypoxia cycle. Compressed air and N_2 injection into the chambers were regulated by a valve system, automatically operated by customized software (Oxycycler, Huff Technologies Inc.). This protocol was repeated with 80 bouts per day (8 hours) during the light cycle in a 12hr light/dark cycle room, for an average of 21 days. Of note the range was 10-29 days, but internal analysis of pilot 10 day protocol showed no difference from the 21 day protocol and were combined in this study. In the remaining 16 hours, the mice were kept under normoxia condition (21% O_2). Control mice were kept in a replicated chamber under normoxic conditions (21% O_2), 24 hours a day during the same duration as the CIH protocol (Figure 1- figure supplement 2). The mice under control conditions has been published (A. D. Huff et al., 2023).

***In Vivo* Experiments**

The same experimental protocol was performed for all Vglut2cre:Ai32, ChATcre:Ai32, ChATcre:Vglut2FlpO:ChR2 mice. Adult mice were initially anesthetized with 100% O_2 and 1.5% Isoflurane (Aspen Veterinary Resources Ltd, Liberty, MO, USA) for 2-3 minutes in an induction chamber. Once the breathing slowed, they were injected with Urethane (1.5 mg/kg, i.p. Sigma Aldrich, St. Louis, MO, USA) and secured supine on a custom surgical table. Core temperature was maintained through a water heating system (PolyScience, Niles, IL, USA) built into the surgical table. Mice were then allowed to spontaneously breathe 100% O_2 for the remainder of the surgery and experimental protocol. Adequate depth of anesthesia was determined via heart and breathing rate, as well as lack of toe pinch response every 15 minutes. A supplemental dose of 0.1mL of Urethane was given to maintain adequate anesthetic depth, when necessary. Bipolar electromyograms (EMG) electrodes were placed in the costal diaphragm to monitor respiratory rate and heart rate throughout the experiment. The trachea was exposed through a midline incision and cannulated caudal to the larynx with a curved (180 degree) tracheal tube (PTFE 24 G, Component Supply, Sparta, TN, USA). The hypoglossal (XII) and vagus (X) nerves were then dissected followed by cannulation of the trachea. The recurrent laryngeal nerve (RLN) was carefully dissected away from each side of the trachea before the cannula was tied in and sealed with super glue to ensure no damage to the RLN. The trachea and esophagus were then cut to detach the rostral end of the trachea just caudal to the cricoid cartilage, preserving the arytenoids and bilateral RLN. A tube filled with 100% O_2 was attached to the cannulated trachea to provide supplemental oxygen throughout the experiment. Continuing in the supine position, the occipital bone was removed, followed by continuous perfusion of the ventral medullary surface with warmed (~36ºC) artificial cerebral spinal fluid (aCSF; in mM: 118 NaCl, 3 KCl, 25 $NaHCO_3$, 1 NaH_2PO_4, 1 $MgCl_2$, 1.5 $CaCl_2$, 30 D-glucose) equilibrated with carbogen (95% O_2, 5% CO_2) by a peristaltic pump (Dynamax RP-1, Rainin Instrument Co; Emeryville CA, USA). As previously published (Fig. 6a (A. Huff et al., 2022)), the XII and X nerves were isolated unilaterally, cut distally, and their activity was recorded from a fire-polished pulled borosilicate glass tip (B150-86-15, Sutter Instrument; Novato, CA, USA) filled with aCSF connected to the monopolar suction electrode (A-M Systems, Sequim, WA, USA) and held in a 3D micromanipulator (Narishige, Tokyo, Japan) (Fig. 7). Multiple bipolar EMGs, using 0.002”

and 0.003” coated stainless steel wires (A-M Systems, Sequim, WA, USA, part no.790600 and 79100 respectively), simultaneously recorded activity from several swallow and respiratory-related muscle sites. According to the techniques of Basmajian and Stecko (J. V. Basmajian & Stecko, 1962), the electrodes were placed using hypodermic needles 30G (part no 305106, BD Precision Glide ™, Franklin Lakes, NJ, USA) in the *submental complex,* which consists of the geniohyoid, mylohyoid and anterior digastric muscles, to determine swallow activity. The *laryngeal complex,* consisting of the posterior cricoarytenoid, lateral, transverse and oblique arytenoid, cricothyroid and thyroarytenoid muscles, to determine laryngeal activity during swallow, as well as postinspiratory activity (Figure 1-figure supplement 2C). The *costal diaphragm*, used to measure the multifunctional activity for both inspiration, as well as *Schluckatmung*, a less common diaphragmatic activation during swallow activity. Glass fiber optic (200 um diameter) connected to a blue (447 nm) laser and DPSS driver (Opto Engine LLC, Salt Lake City, Utah, USA) was placed bilaterally in light contact with the ventral surface of the brainstem overtop of the predetermined PiCo (Anderson et al., 2016) (Fig. 7). At the end of the experiment mice were euthanized by an overdose of anesthetic followed by rapid decapitation or trans-cardial perfusion (see histology section below).

Stimulation protocols

1) Swallow was stimulated by injecting 0.1cc of water into the mouth using a 1.0 cc syringe connected to a polyethylene tube. 2) 25 pulses of each 40ms, 80ms, 120ms, 160ms and 200ms continuous TTL laser stimulation at PiCo was repeated, at random, throughout the respiratory cycle. The lasers were each set to 0.75mW and triggered using Spike2 software (Cambridge Electronic Design, Cambridge, UK). These stimulation protocols were performed in all ChATcre:Ai32, Vglut2cre:Ai32, and ChATcre:Vglut2FlpO:ChR2.

Analysis

All electroneurogram (ENG) and EMG activity were amplified and band-pass filtered (0.03 – 1 KHz) by a differential AC Amplifier (A-M System model 1700, Sequim, WA, USA), acquired in an A/D converter (CED 1401; Cambridge Electronic Design, Cambridge, UK) and stored using Spike2 software (Cambridge Electronic Design, Cambridge, UK). Using the Spike2

software, data was further processed using a band pass filtered (200-700Hz, 40Hz transition gap) then rectified and smoothed (20ms). Using the Spike2 software, the ECGdelete 02.s2s script is used to remove heart artifact, when present, from the ENG and EMG recordings.

We evaluated swallows that were trigged by injection of water into the mouth as well as behaviors in response to laser stimulation applied to the PiCo region: swallow, laryngeal activation and no motor response. Swallow was characterized as a delayed response to the laser outlasting and independent of the laser duration, activation of XII, X, submental and laryngeal complex. Diaphragm activity during PiCo-triggered swallows (*schluckatmung*) was present in some animals but this was not common. Laryngeal activation was characterized as activity of the XII, X, and laryngeal complex dependent on laser pulse duration, and absence of the diaphragm EMG activity. The submental complex was active in a tonic or burst pattern during laryngeal activation. No response was characterized as lack of motor response to the laser and was grouped with laryngeal activation for the non-swallow analysis in respiratory phase shift plots (Figure 3-figure supplement 1). Previously published swallow-related parameters were used to look at swallow-breathing characteristics (Fig.6 (A. Huff et al., 2022)). *Swallow duration* was determined by the onset to the termination of the submental complex EMG activity. In the case the submental complex muscles were not available then it was determined by the onset to the termination of the XII ENG activity. *Swallow sequence* was calculated as the time difference between the peak activation of the laryngeal and submental complex EMG activity. *Schluckatmung* duration was determined by the onset to the termination of the diaphragm EMG activity during a swallow. *Laryngeal activation duration* was determined by the onset to the termination of the laryngeal complex EMG activity. *Diaphragm inter-burst interval* was calculated as the offset of the diaphragm EMG activity to the onset of the subsequent breath. *Inspiratory delay* was calculated as the offset of the swallow-related laryngeal complex EMG activity to the onset of the subsequent breath. Duration and amplitude of each nerve and muscle was determined by the onset to the termination of that respective nerve/muscle activity during swallow. All durations are reported in milliseconds (ms) and all amplitudes are reported as a "% of max" calculated as the % of the maximum baseline (water swallow) amplitude.

As previously reported (Fig. 6d (A. Huff et al., 2022)), respiratory phase reset curves calculated by defining the respiratory cycle as the onset of the diaphragm to the onset of the subsequent diaphragm activity. The *phase shift* elicited by each stimulation of water was

calculated as the duration of the respiratory cycle containing the stimulus, divided by the preceding respiratory cycle. The phase of the swallow stimulation *(respiratory phase)* was calculated as the time between the onset of the inspiration (diaphragm) and the stimulus onset, divided by the expected phase. The average phase shift was then plotted against the respiratory phase in bins containing 1/10 of the expected phase (Baertsch et al., 2018). Swallow histogram plots were created by the phase of breathing in which swallow occurred in, calculated as the onset of inspiration to the onset of swallow divided by the respiratory cycle duration and plotted against the number of swallows that occurred within the 1/10 binned respiratory phase, (*swallow onset: insp onset)*. Swallow was also plotted in relation to the peak activation of the diaphragm as a duration with zero equaling the peak of the inspiratory related diaphragm activity, (*swallow onset: insp peak)*.

Probability plots were calculated by assigning a "0" to the no response behavior or a "0 or 1" to the laryngeal activation or swallow behavior. These numbers were then averaged and plotted against the *respiratory phase* and binned to 1/10 of the respiratory phase.

All data are expressed as mean ± standard deviation (SD), unless otherwise noted. Statistical analyses were performed using GraphPad Prism 9 (GraphPad Software®, Inc. La Jolla, USA). Differences were considered significant at $p \leq 0.05$. Investigators were not blinded during analysis. Sample sizes were chosen on the basis of previous studies.

Histology

At the end of experiments, animals were deeply anesthetized with 5% isoflurane in 100% oxygen and perfused through the ascending aorta with 20 ml of phosphate buffered saline (PB; pH 7.4) followed by 4% phosphate-buffered (0.1 M; pH 7.4; 20 ml) paraformaldehyde (Electron Microscopy Sciences, Fort Washington, PA). The brains were removed and stored in the perfusion fixative for 4 h at 4 °C, followed by 20% sucrose for 8h. Series of coronal sections (25 μm) from the brains were cut using a cryostat and stored in cryoprotectant solution at -20°C (20% glycerol plus 30% ethylene glycol in 50 ml phosphate buffer, pH 7.4) prior to histological processing. All histochemical procedures were done using free-floating sections.

Choline acetyltransferase (*ChAT*) was detected using a polyclonal goat anti-ChAT antibody (AB144P; Millipore; 1:100) and EYFP was detected using a polyclonal mouse anti-GFP (06-896, Millipore; 1:1000) diluted in PB containing 2% normal donkey serum (017-000-121,

Jackson Immuno Research Laboratories) and 0.3% Triton X-100, and incubated for 24 h. Sections were subsequently rinsed in PB and incubated for 2 h in an Alexa 594 donkey anti-goat (705-585-003; 1:250; Jackson Immuno Research Laboratories) and Alexa 488 donkey anti-mouse (715-545-150; 1:250; Jackson Immuno Research Laboratories). For all secondary antibodies used, control experiments confirmed that no labeling was observed when primary antibodies were omitted. The sections were mounted on slides in a rostrocaudal sequential order, dried, and covered with fluoromount (00-4958-02; Thermo Fisher). Coverslips were affixed with nail polish.

Sections were also examined to confirm the transfected cells. *S*ection alignment between specimens was done relative to a reference section. The rostral segment of PiCo was identified by the last section with the caudal end of the facial motor neurons and the first section with the rostral portion of the inferior olives. To distinguish PiCo in each section, we used the nucleus ambiguus (Amb), the inferior olives (IO) and the ventral spinocerebellar tract (vsc) as the main anatomic structures. The section that contains the rostral portion of Amb (more densely packed, i.e. cAmb) is the section that contains the rostral portion of PiCo, in a caudal direction, the compacta portion of Amb turns into a semi-compacta portion (scAmb), being aligned as the zero point in the rostral-caudal graphs. Further caudal, the scAmb turns in the non-compacta portion of Amb (Akins et al., 2017; Baertsch et al., 2018; Kottick et al., 2017; Vann et al., 2018), characterizing the caudal edge of PiCo. PiCo was also anatomically characterized by immunohistological labeling, revealing ChAT-positive neurons located dorsomedial to c-scAmb and caudal to the facial nucleus as previously described (Ain Summan Toor et al., 2019; Anderson et al., 2016). As shown in figure 5 and S1, according to the Paxinos and Franklin mouse atlas (Kirkcaldie et al., 2012), the transfected cells were located slightly dorsal to the NAmb near Bregma level -6.84 mm, ~1100 µm from the midline, and ~700 µm above the marginal layer.

Cell counting, Imaging and Data analysis

A VS120-S6-W Virtual Slide Scanner (Olympus) was used to scan all the sections. Images were taken with a color camera (Nikon DS-Fi3). To restrict any influences on our counted results, the photomicrography and counting were performed by one blind researcher. Image J (version 1.41; National Institutes of Health, Bethesda, MD) was used for cell counting and Canvas software (ACD Systems, Victoria, Canada, v. 9.0) was used for line drawings. A one-in-two series of 25-

µm brain sections was used per mouse, which means that each section analyzed was 50 µm apart. The area analyzed was delimited based on previously reports (Anderson et al., 2016) (mean of 5,423 μm^2). The sections were counted bilaterally, averaged and the numbers reported as mean ± standard error of the mean (SEM). Section alignment were relative to a reference section, as previously described (Anderson et al., 2016) and based on Paxinos and Franklin (Kirkcaldie et al., 2012).

Acknowledgements
We are grateful to receive the NIH grants P01 HL14454 and Project 2 (awarded to J.M.R) HL144801 (awarded to J.M.R.), R01 HL151389 (awarded to J.M.R.), F32 HL160102-01 (awarded to A.H.) for funding this project.

Competing Interest Statement: The authors declare no conflict of interest.

Data Availability: All data is publicly available

Ain Summan Toor, R. U., Sun, Q.-J., Kumar, N., Le, S., Hildreth, C., Phillips, J., & McMullan, S. (2019). Neurons in the intermediate reticular nucleus coordinate post-inspiratory activity, swallowing, and respiratory-sympathetic coupling in the rat. *The Journal of Neuroscience*, 0502-0519. doi:10.1523/jneurosci.0502-19.2019

Akins, V. T., Weragalaarachchi, K., Picardo, M. C. D., Revill, A. L., & Del Negro, C. A. (2017). Morphology of Dbx1 respiratory neurons in the preBötzinger complex and reticular formation of neonatal mice. *Scientific data, 4*(1), 1-9.

Altschuler, S. M., Bao, X., Bieger, D., Hopkins, D. A., & Miselis, R. R. (1989). Viscerotopic representation of the upper alimentary tract in the rat: sensory ganglia and nuclei of the solitary and spinal trigeminal tracts. *Journal of Comparative Neurology, 283*(2), 248-268.

Ambalavanar, R., Tanaka, Y., Selbie, W. S., & Ludlow, C. L. (2004). Neuronal activation in the medulla oblongata during selective elicitation of the laryngeal adductor response. *J Neurophysiol, 92*(5), 2920-2932.

Anderson, T. M., Garcia, A. J., 3rd, Baertsch, N. A., Pollak, J., Bloom, J. C., Wei, A. D., . . . Ramirez, J.-M. (2016). A novel excitatory network for the control of breathing. *Nature, 536*(7614), 76-80. doi:10.1038/nature18944

Arias-Cavieres, A., Fonteh, A., Castro-Rivera, C. I., & Garcia III, A. J. (2021). Intermittent Hypoxia causes targeted disruption to NMDA receptor dependent synaptic plasticity in area CA1 of the hippocampus. *Exp Neurol, 344*, 113808.

Arias-Cavieres, A., Khuu, M. A., Nwakudu, C. U., Barnard, J. E., Dalgin, G., & Garcia, A. J. (2020). A HIF1a-dependent pro-oxidant state disrupts synaptic plasticity and impairs spatial memory in response to intermittent hypoxia. *eNeuro, 7*(3).

Badran, D. H., Al-Hadidi, M. T., Ramadan, H. N., & Abu-Ghaida, J. H. (2005). Location of the motoneurons of the mylohyoid muscle in the rat. A fluorescence and Nissl study. *Neurosciences (Riyadh), 10*(1), 85-89.

Baertsch, N. A., Baertsch, H. C., & Ramirez, J. M. (2018). The interdependence of excitation and inhibition for the control of dynamic breathing rhythms. *Nature communications, 9*(1), 843.

Basmajian, J., & Dutta, C. (1961). Electromyography of the pharyngeal constrictors and levator palati in man. *The Anatomical Record, 139*(4), 561-563.

Basmajian, J. V., & Stecko, G. (1962). A new bipolar electrode for electromyography. *Journal of Applied Physiology, 17*(5), 849-849.

Bhutada, A. M., Broughton, W. A., & Garand, K. L. F. (2020). Obstructive sleep apnea syndrome (OSAS) and swallowing function—a systematic review. *Sleep and Breathing*, 1-9.

Bieger, D., & Neuhuber, W. (2006). Neural circuits and mediators regulating swallowing in the brainstem. *GI Motility online*.

Bonsignore, M. R., Baiamonte, P., Mazzuca, E., Castrogiovanni, A., & Marrone, O. (2019). Obstructive sleep apnea and comorbidities: a dangerous liaison. *Multidisciplinary respiratory medicine, 14*(1), 1-12.

Brockmann, P. E., & Gozal, D. (2022). Neurocognitive Consequences in Children with Sleep Disordered Breathing: Who Is at Risk? *Children (Basel), 9*(9). doi:10.3390/children9091278

Chang, J. L., Goldberg, A. N., Alt, J. A., Mohammed, A., Ashbrook, L., Auckley, D., . . . Rosen,

I. M. (2023). International Consensus Statement on Obstructive Sleep Apnea. *Int Forum Allergy Rhinol, 13*(7), 1061-1482. doi:10.1002/alr.23079

da Silva, M. P., Magalhães, K. S., de Souza, D. P., & Moraes, D. J. A. (2021). Chronic intermittent hypoxia increases excitability and synaptic excitation of protrudor and retractor hypoglossal motoneurones. *J Physiol, 599*(6), 1917-1932. doi:10.1113/jp280788

Dempsey, J. A., Veasey, S. C., Morgan, B. J., & O'Donnell, C. P. (2010). Pathophysiology of sleep apnea. *Physiol Rev, 90*(1), 47-112.

Domingos-Souza, G., Martinez, D., Sinkler, S., Heesch, C. M., & Kline, D. D. (2021). Alpha adrenergic receptor signaling in the hypothalamic paraventricular nucleus is diminished by the chronic intermittent hypoxia model of sleep apnea. *Exp Neurol, 335*, 113517.

Doty, R. W., & Bosma, J. F. (1956). An electromyographic analysis of reflex deglutition. *J Neurophysiol, 19*(1), 44-60. doi:10.1152/jn.1956.19.1.44

Garand, K. L., Strange, C., Paoletti, L., Hopkins-Rossabi, T., & Martin-Harris, B. (2018). Oropharyngeal swallow physiology and swallowing-related quality of life in underweight patients with concomitant advanced chronic obstructive pulmonary disease. *International journal of chronic obstructive pulmonary disease, 13*, 2663-2671. doi:10.2147/COPD.S165657

Garcia, A. J., 3rd, Dashevskiy, T., Khuu, M. A., & Ramirez, J.-M. (2017). Chronic Intermittent Hypoxia Differentially Impacts Different States of Inspiratory Activity at the Level of the preBötzinger Complex. *Frontiers in Physiology, 8*, 571-571. doi:10.3389/fphys.2017.00571

Garcia, A. J., 3rd, Zanella, S., Dashevskiy, T., Khan, S. A., Khuu, M. A., Prabhakar, N. R., & Ramirez, J.-M. (2016). Chronic Intermittent Hypoxia Alters Local Respiratory Circuit Function at the Level of the preBötzinger Complex. *Frontiers in neuroscience, 10*, 4-4. doi:10.3389/fnins.2016.00004

Ghannouchi, I., Speyer, R., Doma, K., Cordier, R., & Verin, E. (2016). Swallowing function and chronic respiratory diseases: systematic review. *Respiratory Medicine, 117*, 54-64.

Horner, R. L. (2023). Targets for obstructive sleep apnea pharmacotherapy: principles, approaches, and emerging strategies. *Expert Opin Ther Targets*, 1-18. doi:10.1080/14728222.2023.2240018

Huff, A., Karlen-Amarante, M., Pitts, T., & Ramirez, J. M. (2022). Optogenetic stimulation of pre–Bötzinger complex reveals novel circuit interactions in swallowing–breathing coordination. *Proceedings of the National Academy of Sciences, 119*(29), e2121095119.

Huff, A. D., Amarante, M. K., Oliveira, L. M., & Ramirez, J.-M. (2023). Role of the postinspiratory complex in regulating swallow-breathing coordination and other laryngeal behaviors. *Elife, 12*, e86103.

Ikari, T., & Sasaki, C. T. (1980). Glottic closure reflex: control mechanisms. *Annals of Otology, Rhinology & Laryngology, 89*(3), 220-224.

Iturriaga, R. (2023). Carotid body contribution to the physio-pathological consequences of intermittent hypoxia: role of nitro-oxidative stress and inflammation. *J Physiol*. doi:10.1113/jp284112

Jean, A. (1984). Control of the central swallowing program by inputs from the peripheral receptors. A review. *Journal of the autonomic nervous system, 10*(3-4), 225-233.

Jia, S., Rybalchenko, N., Kunwar, K., Farmer Jr, G. E., Little, J. T., Toney, G. M., & Cunningham, J. T. (2022). Chronic intermittent hypoxia enhances glycinergic inhibition in nucleus tractus solitarius. *J Neurophysiol, 128*(6), 1383-1394.

Kato, T., Abe, K., Mikami, A., Sugita, H., Muraki, H., Okura, M., . . . Taniguchi, M. (2016). Subjective oropharyngeal symptoms for abnormal swallowing in Japanese patients with obstructive sleep apnea syndrome: a descriptive questionnaire study. *CRANIO®, 34*(2), 95-99.

Kemplay, S., & Cavanagh, J. B. (1983). Bilateral innervation of the anterior digastric muscle by trigeminal motor neurons. *J Anat, 136*(Pt 2), 417-423.

Kessler, J., & Jean, A. (1985). Identification of the medullary swallowing regions in the rat. *Exp Brain Res, 57*(2), 256-263.

Kessler, J. P., & Jean, A. (1985). Inhibition of the swallowing reflex by local application of serotonergic agents into the nucleus of the solitary tract. *Eur J Pharmacol, 118*(1-2), 77-85.

Kirkcaldie, M., Watson, C., Paxinos, G., & Franklin, K. (2012). *Straightening out the mouse neocortex.* Paper presented at the Australian Neuroscience Society Annual Conference.

Kline, D. D. (2010). Chronic intermittent hypoxia affects integration of sensory input by neurons in the nucleus tractus solitarii. *Respiratory physiology & neurobiology, 174*(1-2), 29-36.

Kline, D. D., Ramirez-Navarro, A., & Kunze, D. L. (2007). Adaptive depression in synaptic transmission in the nucleus of the solitary tract after in vivo chronic intermittent hypoxia: evidence for homeostatic plasticity. *J Neurosci, 27*(17), 4663-4673. doi:10.1523/jneurosci.4946-06.2007

Kline, D. D., Wang, S., & Kunze, D. L. (2019). TRPV1 channels contribute to spontaneous glutamate release in nucleus tractus solitarii following chronic intermittent hypoxia. *J Neurophysiol, 121*(3), 881-892.

Kottick, A., Martin, C. A., & Del Negro, C. A. (2017). Fate mapping neurons and glia derived from Dbx1-expressing progenitors in mouse preBötzinger complex. *Physiological reports, 5*(11), e13300.

Kubin, L. (2019). Interactions Between Sleep and Breathing *Handbook of Behavioral Neuroscience* (Vol. 30, pp. 205-221): Elsevier.

Kurnool, S., McCowen, K. C., Bernstein, N. A., & Malhotra, A. (2023). Sleep Apnea, Obesity, and Diabetes - an Intertwined Trio. *Curr Diab Rep, 23*(7), 165-171. doi:10.1007/s11892-023-01510-6

Levring Jaghagen, E., Franklin, K., & Isberg, A. (2003). Snoring, sleep apnoea and swallowing dysfunction: a videoradiographic study. *Dentomaxillofacial Radiology, 32*(5), 311-316.

Lin, M., Liu, R., Gozal, D., Wead, W. B., Chapleau, M. W., Wurster, R., & Cheng, Z. (2007). Chronic intermittent hypoxia impairs baroreflex control of heart rate but enhances heart rate responses to vagal efferent stimulation in anesthetized mice. *American Journal of Physiology-Heart and Circulatory Physiology, 293*(2), H997-H1006.

Ludlow, C. L., Van Pelt, F., & Koda, J. (1992). Characteristics of late responses to superior laryngeal nerve stimulation in humans. *Annals of Otology, Rhinology & Laryngology, 101*(2), 127-134.

Ludlow, C. L., Yamashita, T., Schulz, G. M., & Deleyiannis, F. W.-B. (1995). Abnormalities in long latency responses to superior laryngeal nerve stimulation in adductor spasmodic dysphonia. *Annals of Otology, Rhinology & Laryngology, 104*(12), 928-935.

Marciante, A. B., Shell, B., Farmer, G. E., & Cunningham, J. T. (2021). Role of angiotensin II in chronic intermittent hypoxia-induced hypertension and cognitive decline. *American Journal of Physiology-Regulatory, Integrative and Comparative Physiology, 320*(4), R519-R525.

McNicholas, W. T., Luo, Y., & Zhong, N. (2015). Sleep apnoea: a major and under-recognised public health concern. *J Thorac Dis, 7*(8), 1269-1272. doi:10.3978/j.issn.2072-1439.2015.07.29

Mezzanotte, W. S., Tangel, D. J., & White, D. P. (1992). Waking genioglossal electromyogram in sleep apnea patients versus normal controls (a neuromuscular compensatory mechanism). *The Journal of clinical investigation, 89*(5), 1571-1579.

Nagami, S., Oku, Y., Yagi, N., Sato, S., Uozumi, R., Morita, S., . . . Muro, S. (2017). Breathing–swallowing discoordination is associated with frequent exacerbations of COPD. *BMJ Open Respiratory Research, 4*(1), e000202. doi:10.1136/bmjresp-2017-000202

Nguyen, A. T. D., Jobin, V., Payne, R., Beauregard, J., Naor, N., & Kimoff, R. J. (2005). Laryngeal and velopharyngeal sensory impairment in obstructive sleep apnea. *Sleep, 28*(5), 585-593.

Pack, A. I. (2023). Unmasking Heterogeneity of Sleep Apnea. *Sleep Med Clin, 18*(3), 293-299. doi:10.1016/j.jsmc.2023.05.003

Peng, Y.-J., & Prabhakar, N. R. (2004). Effect of two paradigms of chronic intermittent hypoxia on carotid body sensory activity. *Journal of Applied Physiology, 96*(3), 1236-1242.

Peng, Y.-J., Su, X., Wang, B., Matthews, T., Nanduri, J., & Prabhakar, N. R. (2021). Role of olfactory receptor78 in carotid body-dependent sympathetic activation and hypertension in murine models of chronic intermittent hypoxia. *J Neurophysiol, 125*(6), 2054-2067.

Phillipson, E. A. (1993). Sleep apnea--a major public health problem. *N Engl J Med, 328*(17), 1271-1273. doi:10.1056/nejm199304293281712

Pitts, T., & Iceman, K. E. (2023). Deglutition and the regulation of the swallow motor pattern. *Physiology, 38*(1), 10-24.

Pizzorni, N., Radovanovic, D., Pecis, M., Lorusso, R., Annoni, F., Bartorelli, A., . . . Santus, P. (2021). Dysphagia symptoms in obstructive sleep apnea: prevalence and clinical correlates. *Respiratory research, 22*(1), 1-10.

Prabhakar, N. R., Peng, Y. J., & Nanduri, J. (2023). Carotid body hypersensitivity in intermittent hypoxia and obtructive sleep apnoea. *J Physiol*. doi:10.1113/jp284111

Ramirez, J.-M., Karlen-Amarante, M., Wang, J.-D. J., Bush, N. E., Carroll, M. S., Weese-Mayer, D. E., & Huff, A. (2020). The pathophysiology of rett syndrome with a focus on breathing dysfunctions. *Physiology, 35*(6), 375-390.

Ramirez, J. M., Garcia, A. J., 3rd, Anderson, T. M., Koschnitzky, J. E., Peng, Y. J., Kumar, G. K., & Prabhakar, N. R. (2013). Central and peripheral factors contributing to obstructive sleep apneas. *Respir Physiol Neurobiol, 189*(2), 344-353. doi:10.1016/j.resp.2013.06.004

Razlan, A. N. B., Ullah, M., Kapitonova, M. Y., Liaqat Ali Khan, N. B., & Fuad, S. (2018). Localization of the motor neuron somata of geniohyoid muscle in rat: A horseradish peroxidase study. *Anat Histol Embryol, 47*(5), 410-416. doi:10.1111/ahe.12372

Roberts, E. G., Raphelson, J. R., Orr, J. E., LaBuzetta, J. N., & Malhotra, A. (2022). The Pathogenesis of Central and Complex Sleep Apnea. *Curr Neurol Neurosci Rep, 22*(7), 405-412. doi:10.1007/s11910-022-01199-2

Saboisky, J. P., Stashuk, D. W., Hamilton-Wright, A., Carusona, A. L., Campana, L. M., Trinder, J., . . . White, D. P. (2012). Neurogenic changes in the upper airway of patients with obstructive sleep apnea. *Am J Respir Crit Care Med, 185*(3), 322-329.

Sánchez-de-la-Torre, M., Cubillos, C., Veatch, O. J., Garcia-Rio, F., Gozal, D., & Martinez-Garcia, M. A. (2023). Potential Pathophysiological Pathways in the Complex Relationships between OSA and Cancer. *Cancers (Basel), 15*(4).

doi:10.3390/cancers15041061
Schindler, A., Mozzanica, F., Sonzini, G., Plebani, D., Urbani, E., Pecis, M., & Montano, N. (2014). Oropharyngeal dysphagia in patients with obstructive sleep apnea syndrome. *Dysphagia, 29*(1), 44-51.
Sessle, B. J. (1973). Excitatory and inhibitory inputs to single neurones in the solitary tract nucleus and adjacent reticular formation. *Brain Res, 53*(2), 319-331.
Souza, G. M., Barnett, W. H., Amorim, M. R., Lima-Silveira, L., Moraes, D. J., Molkov, Y. I., & Machado, B. H. (2019). Pre-and post-inspiratory neurons change their firing properties in female rats exposed to chronic intermittent hypoxia. *Neuroscience, 406*, 467-486.
Sun, Q.-J., Chum, J. M., Bautista, T. G., Pilowsky, P. M., & Berkowitz, R. G. (2011). Neuronal mechanisms underlying the laryngeal adductor reflex. *Annals of Otology, Rhinology & Laryngology, 120*(11), 755-760.
Teramoto, S., Sudo, E., Matsuse, T., Ohga, E., Ishii, T., Ouchi, Y., & Fukuchi, Y. (1999). Impaired swallowing reflex in patients with obstructive sleep apnea syndrome. *Chest, 116*(1), 17-21.
Thompson, D. M., Rutter, M. J., Willging, J. P., Rudolph, C. D., & Cotton, R. T. (2005). Altered laryngeal sensation: a potential cause of apnea of infancy. *Annals of Otology, Rhinology & Laryngology, 114*(4), 258-263.
Valbuza, J. S., de Oliveira, M. M., Zancanella, E., Conti, C. F., Prado, L. B. F., Carvalho, L. B., & do Prado, G. F. (2011). Swallowing dysfunction related to obstructive sleep apnea: a nasal fibroscopy pilot study. *Sleep and Breathing, 15*(2), 209-213.
Vann, N. C., Pham, F. D., Dorst, K. E., & Del Negro, C. A. (2018). Dbx1 Pre-Bötzinger Complex Interneurons Comprise the Core Inspiratory Oscillator for Breathing in Unanesthetized Adult Mice. *eNeuro, 5*(3), ENEURO.0130-0118.2018. doi:10.1523/ENEURO.0130-18.2018
Vgontzas, A. N., Karagkouni, E., He, F., Li, Y., Karataraki, M., Fernandez-Mendoza, J., & Bixler, E. O. (2023). Mild-to-moderate obstructive sleep apnea and mortality risk in a general population sample: The modifying effect of age and cardiovascular/cerebrovascular comorbidity. *Journal of Sleep Research*, e13944.
Walshe, M. (2014). Oropharyngeal dysphagia in neurodegenerative disease. *J Gastroenterol Hepatol Res, 3*(10), 1265-1271.
Wright, J., & Sheldon, T. (1998). Sleep apnoea and its impact on public health. *Thorax, 53*(5), 410-413. doi:10.1136/thx.53.5.410

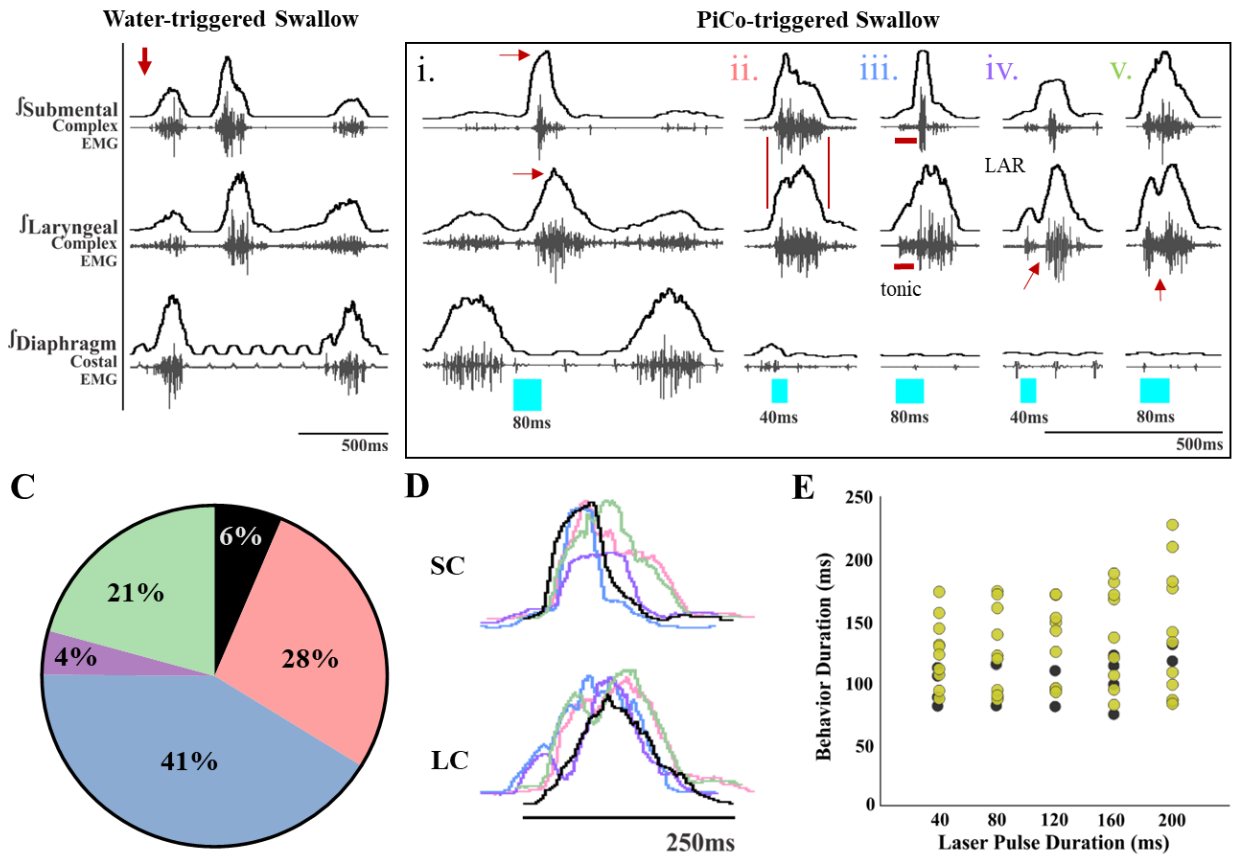

Figure 1

Optogenetic stimulation of PiCo specific ChATcre:Vglut2FlpO:ChR2 neurons triggers variable swallow motor patterns in mice exposed to chronic intermittent hypoxia (CIH). (A) Representative trace of water triggered swallow. (B) Representative traces of PiCo triggered swallows: (Bi) "classic" swallow with the preserved rostrocaudal sequence shown in the red arrows. (Bii) "non-classic" swallow with similar onset, offset and loss of sequence in submental and laryngeal complexes. (Biii) "Tonic" pre-swallow activity with preserved rostrocaudal sequence and low tonic submental and laryngeal activity during the laser pulse, converging into a swallow. (Biv) "Laryngeal Adductor Reflex" (LAR) (purple arrow) followed by a swallow. There is a period of quiescent activity between the LAR and swallow (red arrow). (Bv) "Non-LAR" followed by a swallow. There is an absence of quiescent activity between the laryngeal activity and the swallow (red arrow). (C) Percentage of all PiCo triggered swallows (816 total swallows) in ChATcre:Vglut2FlpO:ChR2 mice. Black is classic, pink is non-classic, blue is tonic, purple is LAR, and green is non-LAR. (D) representative traces of submental complex (SC) and laryngeal complex (LC) from the swallows in panel B with color coding the same as panel C. (E) Scatter plot of behavior duration versus laser pulse duration for swallow in ChATcre:Vglut2FlpO:ChR2 mice. Each dot represents the average duration per mouse. The gold dots represent mice exposed to CIH and the black dots are in control mice exposed to room air taken from Figure 3A in (A. D. Huff et al., 2023).

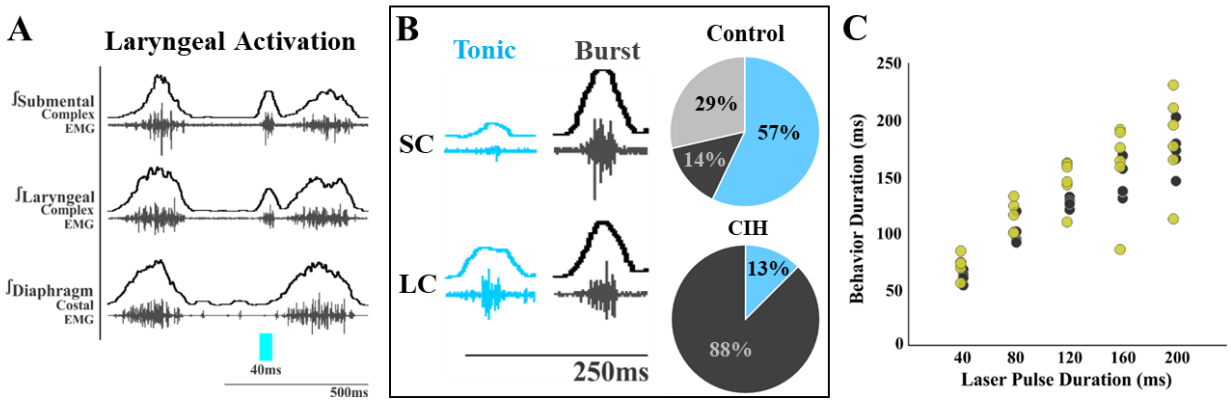

Figure 2.
Optogenetic stimulation of PiCo specific ChATcre:Vglut2FlpO:ChR2 neurons stimulates submental complex burst during laryngeal activation in mice exposed to CIH. (A) Representative traces of PiCo stimulated laryngeal activation with burst pattern submental complex activity. (B) Representative traces of laryngeal activation-related submental complex activity patterns, tonic and burst, and percent of each mouse with the corresponding pattern in control and CIH mice. In control ChATcre:Vglut2FlpO:ChR2 mice, 4 mice had tonic submental complex activity, 1 burst activity and 2 no submental activity. In CIH exposed 1 mouse had tonic activity and 7 burst submental activity. (C) Scatter plot of behavior duration versus laser pulse duration for laryngeal in ChATcre:Vglut2FlpO:ChR2 mice. Each dot represents the average duration per mouse. The gold dots represent mice exposed to CIH and the black dots are in control mice exposed to room air taken from Figure 3A in (A. D. Huff et al., 2023).

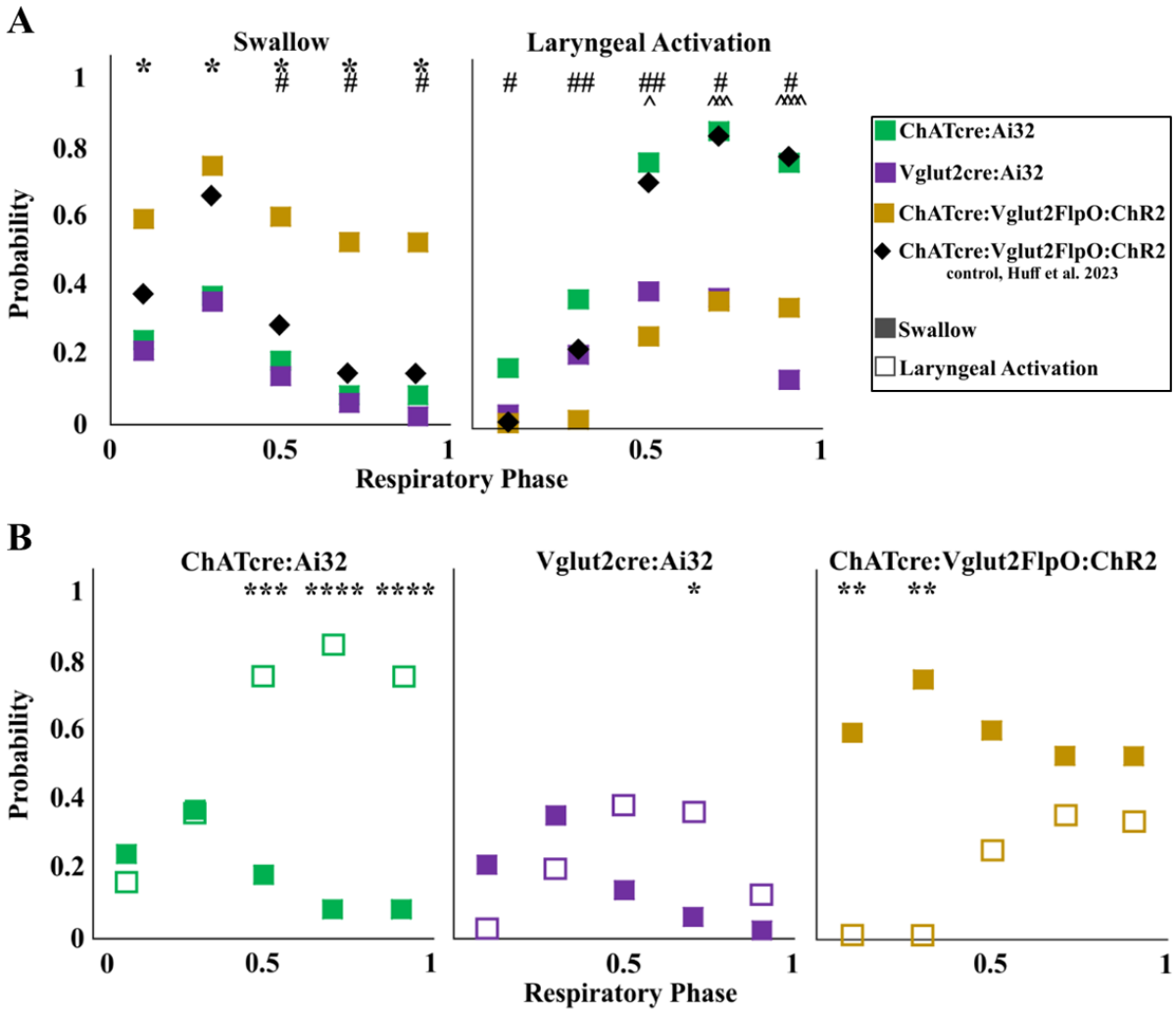

Figure 3.
Optogenetic stimulation of PiCo neurons in mice exposed to CIH regulates swallow and laryngeal activation in a phase-specific manner. A) Scatter plot of the probability of triggering a swallow (left) or laryngeal activation (right) across the respiratory phase (0 start of inspiration, 1 start of next inspiration) in ChATcre:Ai32 mice (green) Vglut2cre:Ai32 mice (purple), ChATcre:Vglut2FlpO:ChR2 mice exposed to CIH (gold), and control ChATcre:Vglut2FlpO:ChR2 mice exposed to room air (black, taken from Figure 1B in (A. D. Huff et al., 2023)) . * Indicates significant difference in probability between Vglut2cre:Ai32 and ChATcre:Vglut2FlpO:ChR2, # Indicates significant difference in probability between ChATcre:Ai32 and ChATcre:Vglut2FlpO:ChR2, and ^ Indicates significant difference in probability between ChATcre:Ai32 and Vglut2cre:Ai32. (B) Scatter plot of the probability of triggering a swallow (closed square) versus laryngeal activation (open square) in all three genetic types exposed to CIH.

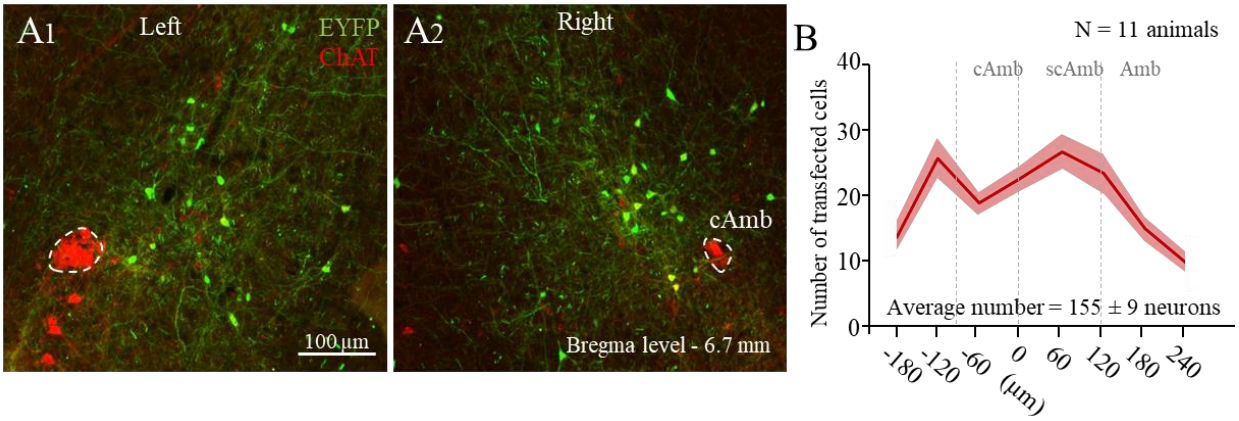

Figure 4.
Transfection of cholinergic/glutamatergic neurons in PiCo in ChATcre:Vglut2FlpO:ChR2 mice. (A) Transverse hemisection through Bregma level (-6.7 mm) of the transfected neurons into PiCo bilaterally, left (A1) and right (A2), with the pAAV-hSyn Con/Fon hChR2(H134R)-EYFP vector. (B) Rostrocaudal distribution of the total number of transfected neurons counted 1:2 series of 25 µm sections into PiCo of 11 animals with an average of 155 ± 9 SEM neurons. Abbreviations: Amb, nucleus ambiguus; cAmb, nucleus ambiguus pars compacta; scAmb, nucleus ambiguus pars semi-compacta.

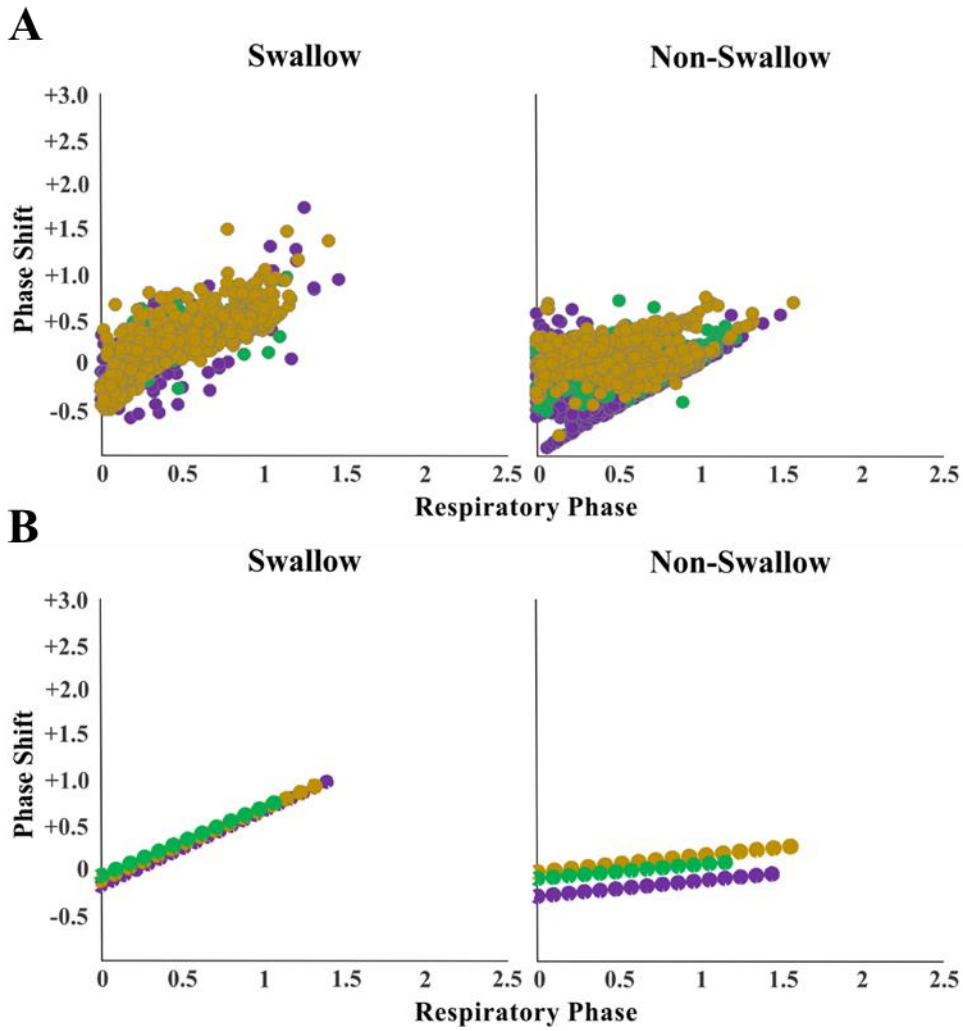

Figure 3 -figure supplement 1

PiCo-triggered swallows reset the respiratory rhythm, while non-swallows have minimal effect, a concept not altered by CIH. Respiratory phase shifts plots were divided into two groups: swallow, PiCo activation that triggered a swallow, or non-swallow, PiCo activation that resulted in laryngeal activation or no motor response. A) Individual responses in ChATcre:Vglut2FlpO:ChR2 (gold), ChATcre:Ai32 (green), and Vglut2cre:Ai32 (purple) mice exposed to CIH and B) line of best fit from the above graphs.

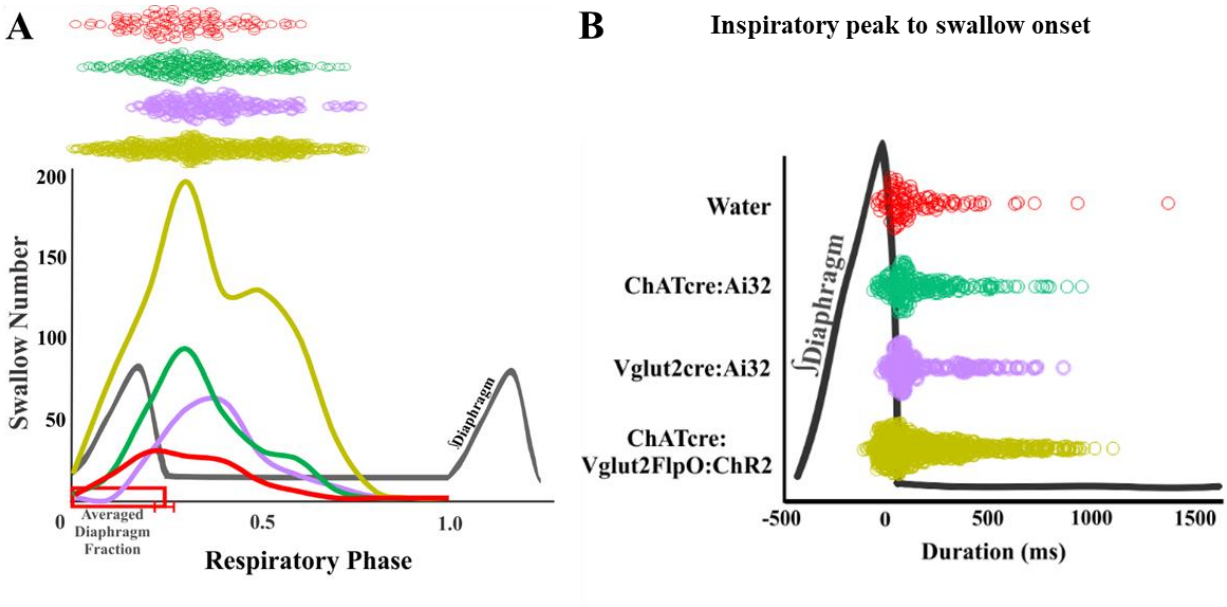

Figure 1- figure supplement 1
No significant differences in swallow-breathing characteristics between water-triggered swallows and PiCo-triggered swallows in mice exposed to CIH. (A) Histogram of swallows in relation to the onset of inspiration for water swallows (red), ChATcre:Ai32 (green), Vglut2cre:Ai32 (purple) and ChATcre:Vglut2FlpO:ChR2 (gold). (B) Dot plot of each swallow in relation to the inspiratory peak. Data for each genetic type is located in supplement table 1.

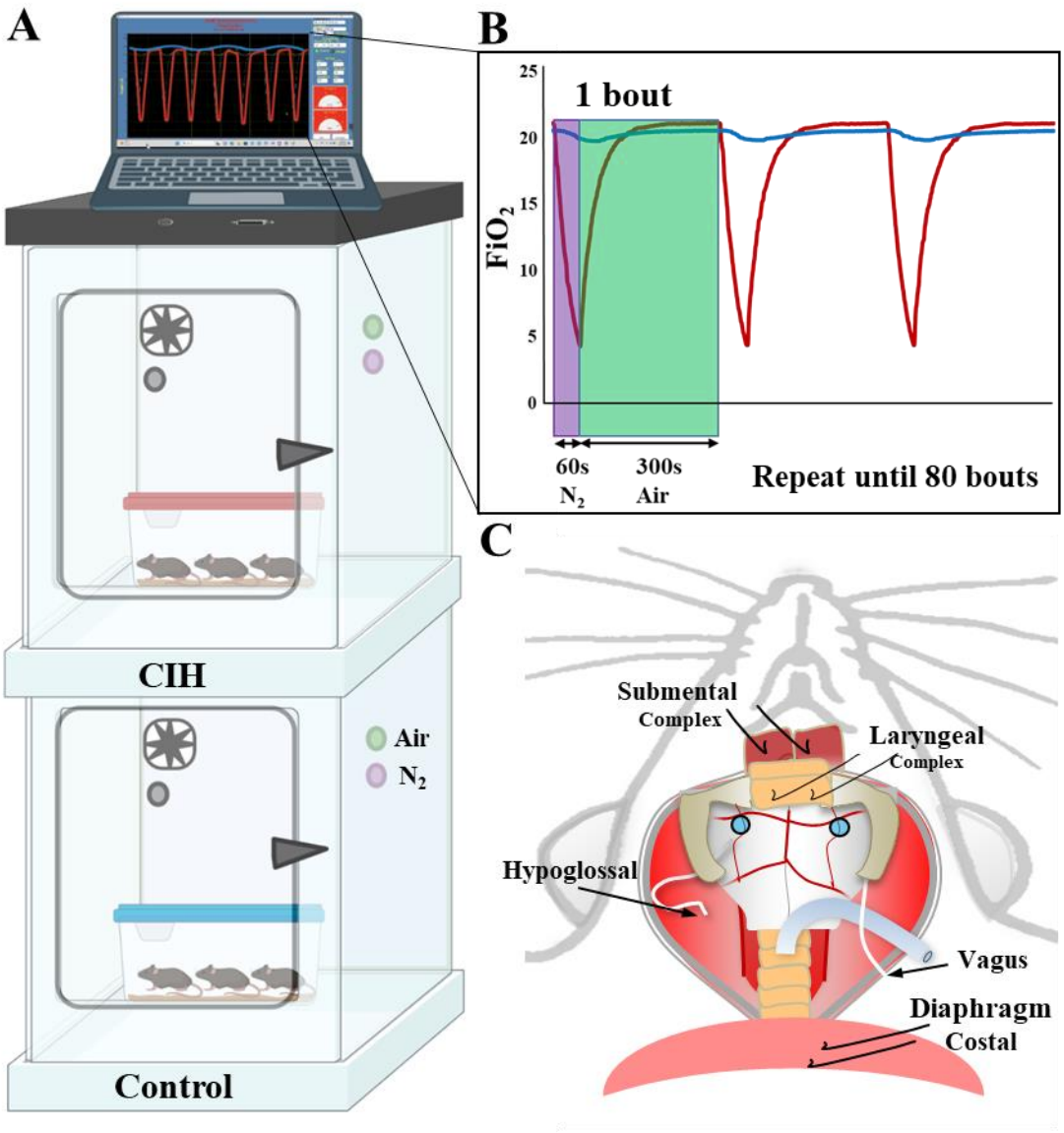

Figure 1- figure supplement 2
Chronic intermittent experimental protocol. (A) Equipment set up for control and CIH protocols. Two plexiglass chambers supplied with a fan, oxygen sensor, and valves for compressed air and Nitrogen. The top chamber serves as the CIH chamber where the oxygen level is automatically controlled by the OxyCycler computer software on top of the chambers. The bottom chamber serves as the control chamber where only air flows through the chamber and the oxygen level is kept at 21% O_2. The mice are kept in their home cage and placed in either chamber for 3 weeks. (B) In the CIH chamber nitrogen (N_2, purple dot) flows into the chamber for 60s, or until the O_2 level reaches 5%. In the event the O_2 level reaches 5% before 60s, no gas flows into the chamber. After 60s, compress air (green dot) flows into the chamber for 5 minutes. These 6 minutes create one bout and is repeated 80 times a day. (C) Graphical depiction of all muscles: submental complex, laryngeal complex and diaphragm; and nerves: hypoglossal and vagus,

recorded to measure swallow and breathing activity. The blue circles depict optrode placement over PiCo.

Supplement Table 1. Provides means, standard deviations (SD), *p*-values, t-statistic (t), degrees of freedom (df), from a paired t-test; and the direction of change for swallow-related parameters when evoked by water (water swallows) and optogenetic stimulation of PiCo in A) ChATcre:Ai32, B) Vglut2cre:Ai32 and C) ChATcre:Vglut2FlpO:ChR2 mice.

A	**Water Swallow**		**+ ChATcre:Ai32 Stimulation**				
	mean	**(SD)**	**mean**	**(SD)**	***p*-value**	**t**	**df**	**Change**
(*n*=14)								
Swallow Duration (ms)	265	(132)	144	(101)	**0.001**	5.21	8	↓
Hypoglossal Duration (ms)	299	(120)	164	(95)	**0.004**	4.07	8	↓
Vagus Duration (ms)	291	(90)	175	(90)	0.05	2.27	8	↓
Laryngeal Complex Duration (ms)	277	(104)	139	(36)	**0.003**	4.42	7	↓
Schluckatmung Duration (ms)	198	(148)	-	(-)	-	-	-	-
Diaphragm Inter-Burst Interval (ms)	637	(184)	588	(179)	0.75	0.34	8	-
SR Inspiratory Delay (ms)	286	(118)	351	(102)	**0.01**	3.14	8	↑
Swallow Sequence (ms)	69	(79)	30	(20)	0.40	0.90	7	-
Swallow Onset: Insp Peak (ms)	122	(90)	144	(88)	0.41	0.87	8	-
Swallow Onset: Insp Onset (0-1 of RC)	0.27	(0.07)	0.32	(0.05)	0.06	2.14	8	-
Hypoglossal Amplitude (% max)	91	(6)	64	(42)	0.06	2.18	8	-
Vagus Amplitude (% max)	95	(5)	62	(35)	**0.03**	2.74	7	↓
Submental Complex Amplitude (% max)	91	(7)	38	(35)	**0.002**	4.91	7	↓
Laryngeal Complex Amplitude (% max)	83	(11)	71	(45)	0.43	0.83	7	-
Schluckatmung Amplitude (% max)	88	(14)	-	(-)	-	-	-	-

B	**Water Swallow**		**+ Vglut2cre:Ai32 Stimulation**				
	mean	**(SD)**	**mean**	**(SD)**	***p*-value**	**t**	**df**	**Change**
(*n*=11)								
Swallow Duration (ms)	308	(184)	125	(44)	**0.0003**	6.46	7	↓
Hypoglossal Duration (ms)	335	(187)	144	(41)	**0.003**	4.59	7	↓
Vagus Duration (ms)	330	(188)	146	(44)	**0.005**	4.09	7	↓
Laryngeal Complex Duration (ms)	380	(238)	155	(46)	**0.004**	4.17	7	↓
Schluckatmung Duration (ms)	119	(75)	87	(12)	0.63	0.66	1	-
Diaphragm Inter-Burst Interval (ms)	827	(526)	459	(246)	**0.01**	3.35	7	↓
SR Inspiratory Delay (ms)	361	(310)	258	(150)	0.26	1.22	7	-
Swallow Sequence (ms)	55	(72)	28	(9)	0.08	2.02	7	-
Swallow Onset: Insp Peak (ms)	171	(113)	131	(91)	0.82	0.24	7	-
Swallow Onset: Insp Onset (0-1 of RC)	0.28	(0.09)	0.38	(0.06)	0.10	1.91	7	-
Hypoglossal Amplitude (% max)	82	(11)	44	(7)	**0.0001**	9.45	7	↓
Vagus Amplitude (% max)	79	(17)	50	(19)	**0.001**	5.13	7	↓
Submental Complex Amplitude (% max)	84	(10)	45	(32)	**0.006**	3.84	7	↓
Laryngeal Complex Amplitude (% max)	86	(11)	64	(34)	0.10	1.87	7	-
Schluckatmung Amplitude (% max)	95	(6)	160	(147)	0.62	0.69	1	-

C	**Water Swallow**		**+ ChATcre:Vglut2FlpO:ChR2 Stimulation**				
	mean	**(SD)**	**mean**	**(SD)**	***p*-value**	**t**	**df**	**Change**
(*n*=11)								
Swallow Duration (ms)	230	(67)	130	(35)	**0.0005**	5.62	8	↓
Hypoglossal Duration (ms)	239	(45)	133	(27)	**0.0003**	6.68	7	↓
Vagus Duration (ms)	256	(62)	140	(37)	**0.0001**	7.11	8	↓
Laryngeal Complex Duration (ms)	260	(58)	144	(34)	**0.0002**	6.66	8	↓
Schluckatmung Duration (ms)	263	(141)	114	(-)	-	-	-	-
Diaphragm Inter-Burst Interval (ms)	786	(327)	711	(345)	0.11	1.79	8	-
SR Inspiratory Delay (ms)	429	(264)	458	(278)	0.55	0.62	8	-
Swallow Sequence (ms)	34	(26)	21	(13)	0.08	1.98	8	-
Swallow Onset: Insp Peak (ms)	175	(95)	188	(151)	0.36	0.98	8	-
Swallow Onset: Insp Onset (0-1 of RC)	0.29	(0.06)	0.34	(0.10)	**0.003**	4.16	8	↑
Hypoglossal Amplitude (% max)	87	(9)	76	(43)	0.47	0.76	7	-
Vagus Amplitude (% max)	87	(7)	58	(32)	**0.01**	3.18	8	↓
Submental Complex Amplitude (% max)	88	(10)	39	(22)	**0.001**	7.47	8	↓
Laryngeal Complex Amplitude (% max)	83	(13)	83	(48)	0.98	0.02	8	-
Schluckatmung Amplitude (% max)	95	(7)	77	(-)	-	-	-	-

Supplement Table 2. Provides means, standard deviations (SD), *p*-values, F value, t-statistic (t), degrees of freedom (df), from a unpaired t-test; and the direction of change for swallow-related parameters between male and female mice during water swallows and PiCo-stimulated swallows in ChATcre:Ai32 mice.

Water Swallow	**Male (*n* =8)**		**Female (*n* =4)**					
	mean	**(SD)**	**mean**	**(SD)**	***p* -value**	**t**	**df**	**Change**
Swallow Duration (ms)	307	(142)	181	(55)	0.13	1.67	10	-
XII Duration (ms)	336	(133)	224	(22)	0.13	1.64	10	-
Vagus Duration (ms)	312	(99)	249	(57)	0.27	1.16	10	-
Laryngeal Complex Duration (ms)	312	(122)	225	(43)	0.21	1.36	8	-
Schluckatmung Duration (ms)	198	(148)	-	(-)	-	-	-	-
Diaphragm Inter-Burst Interval (ms)	655	(181)	601	(213)	0.66	0.46	10	-
SR Inspiratory Delay (ms)	261	(94)	335	(160)	0.33	1.02	10	-
Swallow Sequence (ms)	93	(95)	33	(26)	0.26	1.21	8	-
Swallow Onset: Insp Peak (ms)	135	(86)	94	(105)	0.48	0.74	10	-
Swallow Onset: Insp Onset (0-1 of RC)	0.27	(0.06)	0.27	(0.08)	0.93	0.09	10	-
+ ChATcre:Ai32	**Male (*n* =7)**		**Female (*n* =3)**					
Stimulation	**mean**	**(SD)**	**mean**	**(SD)**	***p* -value**	**t**	**df**	**Change**
Swallow Duration (ms)	154	(118)	122	(55)	0.67	0.44	8	-
XII Duration (ms)	178	(107)	129	(60)	0.48	0.73	8	-
Vagus Duration (ms)	187	(103)	148	(59)	0.57	0.60	8	-
Laryngeal Complex Duration (ms)	135	(30)	147	(54)	0.67	0.44	7	-
Schluckatmung Duration (ms)	-	(-)	-	(-)	-	-	-	-
Diaphragm Inter-Burst Interval (ms)	573	(107)	622	(327)	0.72	0.37	8	-
SR Inspiratory Delay (ms)	340	(59)	377	(187)	0.62	0.51	8	-
Swallow Sequence (ms)	29	(18)	32	(28)	0.83	0.22	7	-
Swallow Onset: Insp Peak (ms)	129	(23)	182	(183)	0.43	0.83	8	-
Swallow Onset: Insp Onset (0-1 of RC)	0.31	(0.04)	0.37	(0.04)	**0.04**	2.38	8	↑

Supplement Table 3. Provides means, standard deviations (SD), *p*-values, F value, t-statistic (t), degrees of freedom (df), from a unpaired t-test; and the direction of change for swallow-related parameters between male and female mice during water swallows and PiCo-stimulated swallows in Vglut2cre:Ai32 mice.

Water Swallow	**Male (*n* =5)**		**Female (*n* =6)**					
	mean	**(SD)**	**mean**	**(SD)**	***p* -value**	**t**	**df**	**Change**
Swallow Duration (ms)	346	(238)	277	(139)	0.56	0.61	9	-
XII Duration (ms)	365	(242)	306	(132)	0.65	0.48	8	-
Vagus Duration (ms)	365	(239)	294	(138)	0.58	0.58	8	-
Laryngeal Complex Duration (ms)	410	(326)	356	(162)	0.73	0.36	9	-
Schluckatmung Duration (ms)	85	(39)	219	(-)	0.10	2.95	2	-
Diaphragm Inter-Burst Interval (ms)	1097	(687)	602	(208)	0.13	1.69	9	-
SR Inspiratory Delay (ms)	542	(399)	211	(72)	0.07	2.02	9	-
Swallow Sequence (ms)	66	(80)	45	(70)	0.66	0.46	9	-
Swallow Onset: Insp Peak (ms)	225	(134)	125	(75)	0.15	1.57	9	-
Swallow Onset: Insp Onset (0-1 of RC)	0.29	(0.13)	0.28	(0.06)	0.97	0.03	9	-
+ Vglut2cre:Ai32	**Male (*n* =3)**		**Female (*n* =5)**					
Stimulation	**mean**	**(SD)**	**mean**	**(SD)**	***p* -value**	**t**	**df**	**Change**
Swallow Duration (ms)	145	(52)	113	(39)	0.36	0.99	6	-
XII Duration (ms)	168	(45)	129	(35)	0.22	1.38	6	-
Vagus Duration (ms)	172	(51)	131	(37)	0.24	1.32	6	-
Laryngeal Complex Duration (ms)	170	(61)	145	(40)	0.49	0.73	6	-
Schluckatmung Duration (ms)	95	(-)	79	(-)	-	-	-	-
Diaphragm Inter-Burst Interval (ms)	584	(281)	384	(218)	0.30	1.14	6	-
SR Inspiratory Delay (ms)	358	(173)	197	(109)	0.15	1.65	6	-
Swallow Sequence (ms)	28	(10)	28	(10)	0.97	0.03	6	-
Swallow Onset: Insp Peak (ms)	141	(99)	125	(97)	0.84	0.22	6	-
Swallow Onset: Insp Onset (0-1 of RC)	0.35	(0.10)	0.40	(0.02)	0.33	1.06	6	-

Supplement Table 4. Provides means, standard deviations (SD), *p*-values, F value, t-statistic (t), degrees of freedom (df), from a unpaired t-test; and the direction of change for swallow-related parameters between male and female mice during water swallows and PiCo-stimulated swallows in ChATcre:Vglut2FlpO:ChR2 mice.

Water Swallow	**Male (*n* =2)**		**Female (*n* =7)**					
	mean	**(SD)**	**mean**	**(SD)**	***p* -value**	**t**	**df**	**Change**
Swallow Duration (ms)	194	(65)	240	(68)	0.43	0.85	7	-
XII Duration (ms)	245	(11)	237	(52)	0.84	0.21	6	-
Vagus Duration (ms)	234	(51)	262	(68)	0.61	0.53	7	-
Laryngeal Complex Duration (ms)	221	(56)	271	(58)	0.33	1.06	7	-
Schluckatmung Duration (ms)	-	(-)	263	(141)	-	-	-	-
Diaphragm Inter-Burst Interval (ms)	1086	(13)	701	(322)	0.15	1.61	7	-
SR Inspiratory Delay (ms)	730	(51)	343	(232)	0.06	2.24	7	-
Swallow Sequence (ms)	8	(7)	41	(25)	0.12	1.79	7	-
Swallow Onset: Insp Peak (ms)	202	(113)	167	(98)	0.68	0.43	7	-
Swallow Onset: Insp Onset (0-1 of RC)	0.26	(0.09)	0.38	(0.05)	**0.04**	2.51	7	↑
+ ChATcre:Vglut2FlpO:ChR2	**Male (*n* =4)**		**Female (*n* =7)**					
Stimulation	**mean**	**(SD)**	**mean**	**(SD)**	***p* -value**	**t**	**df**	**Change**
Swallow Duration (ms)	130	(27)	127	(38)	0.89	0.14	9	-
XII Duration (ms)	128	(33)	137	(26)	0.63	0.50	8	-
Vagus Duration (ms)	138	(42)	139	(36)	0.96	0.05	9	-
Laryngeal Complex Duration (ms)	122	(32)	158	(30)	0.10	1.82	9	-
Schluckatmung Duration (ms)	-	(-)	114	(-)	-	-	-	-
Diaphragm Inter-Burst Interval (ms)	847	(290)	623	(367)	0.32	1.04	9	-
SR Inspiratory Delay (ms)	625	(294)	357	(238)	0.13	1.66	9	-
Swallow Sequence (ms)	13	(6)	22	(12)	0.21	1.34	9	-
Swallow Onset: Insp Peak (ms)	159	(188)	191	(139)	0.75	0.33	9	-
Swallow Onset: Insp Onset (0-1 of RC)	0.26	(0.14)	0.30	(0.05)	0.48	0.74	9	-